Lipoid S-75 + cholesterol + ATO

Organic solvent evaporation

By rotary evaporator

Lipidic thin film formation

Hydrate by glycerol aqueous solution

Glycerosomes dispersion

Sonicate using probe sonicator

Chapter-5

Formulation development of ATO loaded glycerosomes

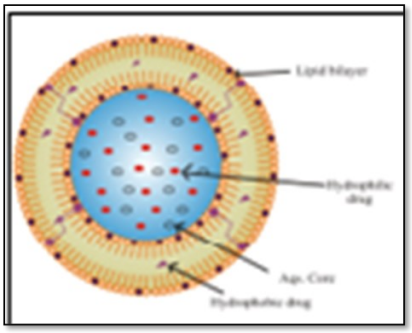

Glycerosomes

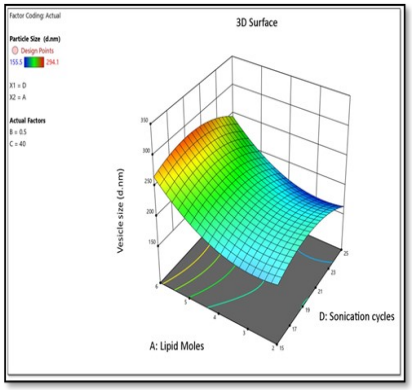

Optimization by DSD

Evaluation of ATO loaded glycerosomes

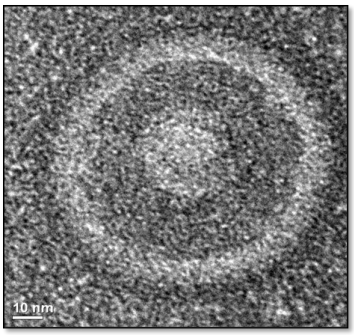

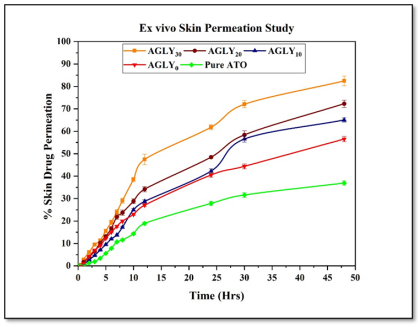

Stability study

5.1. Glycerosomes:

Glycerosomes are novel vesicular drug delivery systems which have been studied widely as potential drug carriers for transdermal drug delivery. Glycerosomes are closed bilayer vesicles composed of phospholipid, cholesterol, and glycerol.

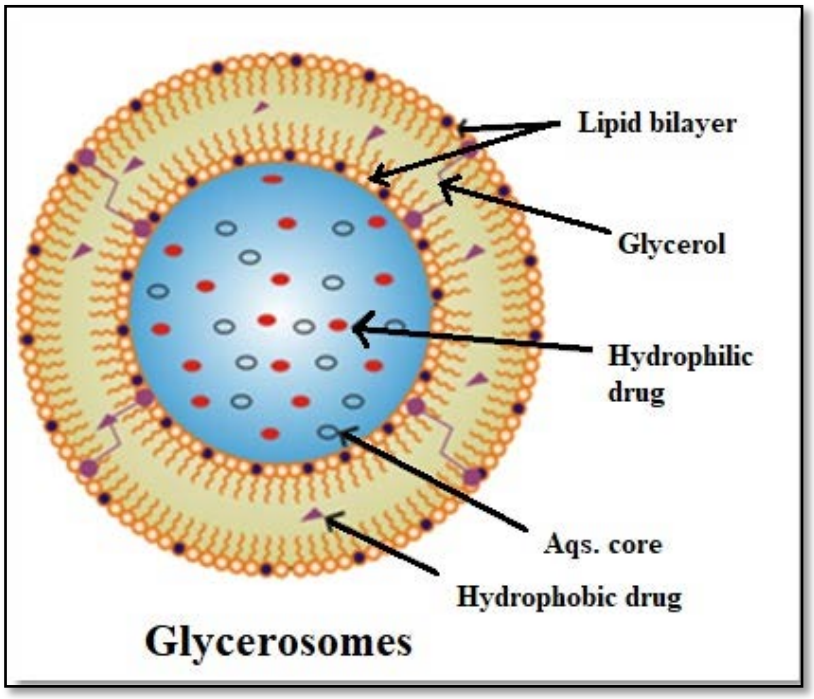

Figure- 5.1. Structure of glycerosomes

In development of glycerosomes, selection of well-suited method for preparation and lipid play an important role. This research work includes preliminary trials which were taken for selection of well-suited method for preparation of glycerosomes. Amongst various available methods, we tried thin film hydration method, and reverse phase solvent evaporation method. Based on lower vesicle size and higher entrapment efficiency, thin film hydration method was used for formulation of glycerosomes. The selection of lipid was major factor affected on vesicle size and entrapment efficiency, amongst several lipids, Lipoid S-75 was showed highest entrapment efficiency and lower vesicle size. Hence, Lipoid S-75 was used as lipid for preparation of glycerosomes. After that, optimization of process parameters and formulation factors were carried out.

5.2. Selection of method for preparation of glycerosomes:

In this present work, we have tried two methods for formulation development of atorvastatin loaded glycerosomes.

1. **Lipidic thin film hydration method:**

   Lipoid S-75, cholesterol (in mole ratio with drug) and ATO was dissolved in organic solvent mixture of chloroform and methanol (1:1 v/v) in 50 ml of round bottom flask. Then organic solvent was evaporated by rotary evaporator under reduced vacuum at 60±5°C for 30 minutes at 150 rpm to form uniform thin layer of lipid phase. The traces of organic solvent were then removed by keeping the film in desiccator under reduced pressure for overnight. The prepared dried thin film was hydrated by glycerol aqueous solution (10mL) at (50°C) for 1 hr at 150 rpm. The obtained dispersion was sonicated with 40 % amplitude (2 sec ON and 2 sec OFF; 25 cycle). Then dispersion was passed through sephadex G-25 column to remove unentrapped drug and stored at 2-8°C for further study [1, 2].

2. **Reverse phase solvent evaporation method:**

   Lipoid S-75, cholesterol (in mole ratio of 4:1 with drug) and atorvastatin were dissolved in methanol: chloroform (in ratio of 1:1), while aqueous phase contains amount of glycerol dissolved in double distilled water. The aqueous phase was added to the organic phase at a ratio of 1:3 (v/v) and sonicated for 30 min in a bath sonicator. The organic solvents were then removed by rotary evaporator to obtain a dry film. The resulting prepared film was hydrated with glycerol aqueous solution and sonicated in an ice water bath on probe sonicator with 40 % amplitude (2 sec ON and 2 sec OFF; 25 cycle). Then dispersion was purified by passing through sephadex G-25 column to remove unentrapped drug. Then, the purified glycerosomes were stored at 2-8°C for further study [3].

From the above available methods, the selection of suitable method for preparation of glycerosomes was based on lower vesicle size and maximum entrapment efficiency.

5.3. Selection of lipids:

By keeping other formulation and process variables constant, different lipids and their combination were tried. Lipoid S-75, Lipoid S-100, DPPC, Phospholipon 90H, DSPC and Phospholipon 80H were used for screening of lipids.

5.4. Drug-Excipients interaction studies by FTIR:

The interaction of pure drug (ATO) with mixture of excipients (lipid and cholesterol) were analysed by FTIR (Bruker, Germany). Thin KBr pellet was prepared and data were collected in the range of 400 to 4000 cm^{-1} to determine compatibility of excipients with drug. (Mentioned in chapter no. 4 – Preformulation study – Section 4.2 and 4.4)

5.5. Identification of independent variables and qualitative risk assessment using Ishikawa diagram

All possible variables which were linked with the development of ATO loaded glycerosomes were demonstrated with the help of Ishikawa diagram. These factors were considered as 'low, moderate and high risk' based on their predicted effect on vesicle size and % EE.

5.6. Optimization:

The various process and formulation variables for preliminary study included speed of rotation for film hydration and film formation, solvent evaporation time, hydration time, hydration volume, hydration medium, lipid:drug molar ratio, cholesterol:drug molar ratio, amplitude of sonication, sonication cycles and glycerol concentration. Amongst these, the lipid:drug molar ratio, cholesterol:drug molar ratio, amplitude of sonication and sonication cycles were found to be more critical variables which showed significant effect on vesicle size and entrapment efficiency. Hence, these were optimized by definitive screening method (response surface methodology).

5.6.1. Optimization of variables:

Following variables were optimized by one factor at a time (OFAT) approach based on minimum vesicle size (VS) and maximum entrapment efficiency (%EE) (shown in table-5.1).

Table- 5.1. Parameter screening and optimization of drug loaded glycerosomes

Variables type	Variables	Screened values/range	
Process variables	**Solvent evaporation time for film formation (min)**	15	45
	Speed of rotation for film formation and hydration (RPM)	50	175
	Vacuum condition (mmHg)	200	500
	Hydration time (min)	30	75
	Pulse of sonication cycle	2 Sec ON, 2 Sec OFF	5 Sec ON, 5 Sec OFF
	Amplitude of sonication (%)	10	70
	Cycle of sonication	10	30
Formulation variables	**Lipid:Drug (Molar ratio)**	2:1	6:1
	Cholesterol:Drug (Molar ratio)	0:1	1.5:1
	Glycerol concentration (% w/w)	10	40
	Hydration volume	5	15
	Hydration medium	Mili-Q water	PBS 7.4

5.6.2. Optimization of ATO loaded glycerosomes by Definitive Screening Design (DSD):

The four variables namely Lipid:drug molar ratio, Cholesterol:drug molar ratio, Amplitude and cycle of sonication were selected as independent factors which were high-risk factors of prepared glycerosomes respect to vesicle size and entrapment efficiency selected as dependent factors. The optimization was done by Definitive Screening Design (DSD) using statistical model and desirability function, while the effect of independent variables on dependent variables was studied and analysed by

software DesignExpert@V13 (Stat-Ease, Inc., USA). Total 13 runs, four factors, three levels DSD design were used to study the effect of independent variables on responses. The summary of independent and dependent variables with the goal set of response are shown in table- 5.2.

Table- 5.2. Variables selected for DSD for optimization of ATO loaded Glycerosomes.

Independent Variables		
Variables	**Low Level**	**High Level**
Lipid:drug molar ratio (A)	2:1	6:1
Cholesterol:drug molar ratio (B)	0:1	1:1
Amplitude (C)	20	60
Cycles of sonication (D)	15	25
Dependent Variables		
Variables	**Goal**	**Importance**
VS (Y1)	Minimize	+++
% EE (Y2)	Maximize	+++

5.6.3. Validation of Check Point Batch:

The check point batch obtained from design was prepared in triplicate and evaluated for vesicle size and entrapment efficiency. The predicted response which was obtained from design was compared with observed response.

5.7. Characterization of glycerosomes:

a. Vesicle size and polydispersity index (PDI):

The average vesicle size and polydispersity index (PDI) were analyzed by dynamic light scattering using Malvern zetasizer Nano-ZS 90 (Malvern Instrument, Worcestershire, United Kingdom). The surface charge was also analyzed by the same equipment in triplicates [4, 5].

b. % Entrapment Efficiency (% EE) and % Drug Loading Capacity (%DLC):

The free ATO was separated by using sephadex G-25 column for determination of entrapment efficiency. The ATO loaded Glycerosomal dispersion was passed through sephadex G-25 column. Distilled water then passed through column to elute sample. Firstly, the vesicular dispersion was eluted from column and after complete elution of vesicular dispersion. Then this fraction was analyzed by UV Visible spectrophotometer at 246 nm [6, 7]. The % EE was calculated as follows:

$$\%EE = \frac{\text{Total ATO added} - \text{Free ATO}}{\text{Total ATO added}} \times 100$$

…….equation- 5.1.

The % drug loading capacity (% DLC) was calculated as follows [8]:

$$\%\text{DLC} = \frac{\text{Amount of ATO in glycerosomes}}{\text{Total solid content}} \times 100$$

…….equation- 5.2.

c. Morphological evaluation:

The morphology of vesicles was confirmed by transmission electron microscopy (TEM) analysis (JEM-2100, 200 kV, Jeol Ltd., Japan). Samples were placed on carbon coated copper grid, stained with phosphotungstic acid (1%) and allowed to stand for drying. The grid was put in a sample probe, then examined under a microscope with a 20-200 kV working voltage range and adequate magnification [3, 9].

d. Residual solvent study:

The residual solvents study was performed by gas chromatography (Perkin Elmer, USA). The standard sample of chloroform (25 µg/mL) and methanol (5 µg/mL) was prepared in DMF. Samples were prepared in similar dilution order of standard for comparison. Using nitrogen as the carrier gas, the sample was injected into the capillary column (CR-624, dimensions: 30 m, 0.53 mm, 3.00 µm) at a temperature of 80°C. Others parameters like carrier gas flow rate, H_2 gas flow rate, air flow rate, injection volume, injector temperature, and detector temperature were set to 40

mL/min, 30 mL/min, 300 mL/min, 0.2 µL, 260°C, and 260°C respectively. Total run time was set at 20 min. 20 minutes was the allotted runtime [10-12].

5.8. Optimization and impact of glycerol concentration on ATO loaded glycerosomes:

The effect of change in concentration of glycerol on physicochemical characteristics, deformability index, *in vitro* drug release and *ex vivo* skin permeation were analyzed. The ATO loaded glycerosomes were prepared by using optimized parameters obtained from design by varying glycerol concentration from 0 to 30% w/w. All-prepared batches were analysed for physicochemical characteristics, *In vitro* drug release and *ex vivo* skin permeation study.

5.8.1. Deformability Index:

Deformability index of glycerosomes was measured by extrusion method. The vesicular dispersion was extruded through polycarbonate filters of pore size of 100 nm at constant pressure. The deformability index was calculated by following equation:

$$DI = J\left[\frac{r_v}{r_p}\right]^2 \qquad \text{.....equation- 5.3.}$$

Where, J is fraction of dispersion collected after extrusion (it is between 0 to 1, in which 0 represents no fraction recovered, while 1 represents 100% of the dispersion recovered), rv is the size of vesicles following extrusion in nm, and rp is the pore size of the barrier (nm) [2].

5.8.2. Rheological study:

The rheological studies were performed using a controlled stress rheometer, rotational rheometer (HAAKE MARS III, Thermo Scientific). The shear dynamic viscosity was measured using parallel plate geometry. The formulation was loaded with a silicon oil layer in between parallel plates to avoid water evaporation during measurement and kept for 10 minutes for temperature stabilization. The rheological outputs were recorded via an electronic box attached to a computer controlled for scanning at room temperature along with a dynamic shear rate of 0 s^{-1} to 30 s^{-1} intervals [13, 14].

5.8.3. *In vitro* drug release study:

1. Activation of dialysis bag:

For the study, a dialysis membrane-130 (la 393) with a molecular weight cut-off of 12000–14000 DA and an estimated capacity of 2.41 mL/cm was used. It was purchased from Himedia Labs Pvt. Ltd., India. To activate the dialysis bag, a 10-cm-long dialysis membrane was cut, placed overnight under running water to remove glycerol, and then treated for one minute with sodium sulphide solution (0.3% w/v) at 80 °C to remove sulphur compounds (s). Moreover, washing was done in hot water at 60 °C. After washing, a step of acidification using 0.2% v/v sulfuric acid was performed, and the acid was then removed by washing with hot water. The dialysis membrane was then incubated in the diffusion medium overnight before the *In vitro* release study [15, 16].

2. *In vitro* drug release:

The *in vitro* drug release from pure ATO and ATO loaded glycerosomes was performed to study the effect of concentration of glycerol on release rate of drug from formulations. Pure ATO and ATO loaded glycerosomes was filled into dialysis bag (MW cut-off of 12k-14k Da) and placed in 50 ml of saline phosphate buffer pH 7.4 as well as PBS pH 5.5 containing 2% of propylene glycol under magnetic stirring at 100 rpm at 37±0.5 °C. The samples were withdrawn from diffusion medium at their predetermined time interval upto 48 hrs and replaced with same amount of freshly prepared diffusion medium to maintain sink condition [17]. The withdrawn samples were analyzed by spectrophotometric method [18].

To describe the release, the release data were fit to several exponential equations, including Zero order, First order, Higuchi, and Korsmeyer-Peppas model [19-22]. These models were fitted to data from drug release study in order to identify the model that best fitted the glycerosomes release profile. The various release kinetic equations are shown in table- 5.3.

Table- 5.3. Various release kinetic models

Model	Equation
Zero order	$Q_0 - Q_t = K_0 t$
First order	$Log\ C = Log\ C_0 - \frac{Kt}{2.303}$
Higuchi	$f_t = Q_t = k_H \sqrt{t}$
Korsmeyer-Peppas	$\frac{M_t}{M_\infty} = K\ t^n$

Where, Q_t is the amount of drug dissolved in time t, Q_0 is the initial amount of drug and K_0 is the zero-order release constant, C_0 is the initial concentration of drug, k is the first order rate constant, Q is the amount of drug released in time t, K_H is the Higuchi dissolution constant, W_0 is the initial amount of drug and M_t is the drug released at time t, M_∞ is the quantity of drug released at infinite time, K is the kinetic constant, and n is an exponent to characterize different release mechanisms [19]. The interpretation of release exponent (n) is shown in table – 5.4.

Table- 5.4. Interpretation of release exponents (n)

Release mechanism Model	Release exponents (n)
Fickian diffusion	0.43
Anomalous transport	0.43 < n <0.85
Case I transport	0.85
Case II transport	n > 0.85

5.8.4. *Ex vivo* skin permeation study:

1. Skin collection and skin preservation:

Rat skin was obtained from the G.H. Patel Pharmacy Building, The Maharaja Sayajirao University of Baroda, Vadodara, Gujarat under the IAEC (Institutional Animal Ethical Committee) with protocol number of MSU/IAEC/2021-22/2110. Sprague Dawley rats (6-8 weeks old, 200-250gm) were euthanized with prolonged ether anaesthesia and the abdominal skin of each rat was excised. Hairs on the stratum corneum of skin was removed by shaving. The isolated rat skin was rinsed

with PBS 7.4, immediately soaked in glycerol solution and preserved into dry ice for transportation to working place. Then skin was thawed in PBS 7.4 at room temperature. Residual adhering fat from dermal side was removed by isopropyl alcohol and washed with phosphate buffer pH 7.4. The skin was then cut into the circular pieces having dimension of Franz diffusion cell with same thickness [23, 24].

2. *Ex vivo* skin permeation and retention study:

The skin specimen was mounted on the Franz diffusion cell such that stratum corneum faced the donor receptor and dermis side faced the receptor compartment. The receptor compartment was filled with phosphate buffer 7.4 containing 2% of propylene glycol at 32 ± 0.5°C under constant magnetic stirring at 100 rpm and under non-occlusive condition. Glycerosomal dispersion containing equivalent amount of ATO were placed in donor compartment. Samples were withdrawn from receptor medium at predetermined time intervals and replaced with freshly prepared PBS 7.4. The withdrawn samples were filtered through 0.45 µm syringe filter and analyzed at 246 nm using UV-Vis spectrophotometrically [25].

The skin was removed from Franz diffusion cell after study completion and the donor side was washed with methanol and collected the washed sample for calculation of drug remained on skin. The skin was then cut into small pieces and suspended into methanol. The suspension was homogenized for 15 min and sonicated using bath sonicator to remove drug which was accumulated into skin layers. After that, the samples were centrifuged for 10 minutes at 5000 rpm. The supernatant was collected and filtered through 0.45 µm syringe filter and analyzed to estimate drug retained in the skin [26-29].

The data obtained were plotted as % cumulative drug permeated through skin as a function of time. The drug remained on skin and retained in skin was calculated. The transdermal flux (Jss, % drug permeated/cm^2/hr) was calculated on the basis of the obtained % drug permeation through skin per hour. The permeation enhancement ratio were calculated as follows [30]:

$$Permeation\ enhancement\ ratio\ = \frac{J_{ss}\ Test}{J_{ss}\ Control}$$

…….equation- 5.4.

5.8.5. *In vitro* cell line studies:

a. Cell culture:

Skin fibroblast cells (3T3) were purchased from NCCS, Pune, India and grown in T-25 cell culture flask incubated in CO_2 incubator in 5% CO2 and 100% humidity at 37°C for 24 Hrs. The culture growth media contained DMEM (high glucose), 10% of foetal bovine serum and 1% of antibiotic solution. After 24 hrs, the culture medium from the flask was removed and adhered cells were washed with sterile PBS 7.4. After washing, the Trypsin-EDTA solution was poured in order to completely cover the surface of the flask, and it was kept in the incubator for 2 minutes at 37°C to detach the adhered cell from the flask. After complete detachment of cells, neutralized the trypsin by adding freshly prepared culture media. The cell dispersion was centrifuged at 1200 rpm for 2 minutes. After centrifugation, the supernatant was discarded and cell pellets were resuspended in fresh growth media. The cells were counted using Neubauer's chamber and transferred into other new cell culture flak with cell density of 1 X 10^4 cells/cm^2. Then, flasks were kept in incubator at 5% CO_2 and 37°C temperature for further cell culture. The growth media was replaced every 48 hrs and passaging was done after 80-90% confluency [31, 32].

b. Cell viability assessment by MTT assay:

The skin fibroblast cells-3T3[33] (7500 cells/well) was seeded in 96-well plates filled with 200 µl of culture growth medium. After 24 hrs, the cells were washed with sterile phosphate buffer 7.4 and replaced with fresh growth medium. Then cells were treated for 12 and 24 hrs with pure drug, placebo formulations (Liposomes and Glycerosomes) and drug loaded formulations (Liposomes and Glycerosomes). Each sample was tested in triplicates. Cells treated with Triton X 100 and PBS 7.4 were used as negative and positive control respectively. After completion of treatment period, the cells were washed with fresh medium at least three times and

add 200 µL of MTT reagent (1mg/mL in PBS) to each well. After 2-3 hrs, formed formazan crystals were dissolved in 100 µL of dimethyl sulfoxide and their concentration was spectrophotometrically quantified at 570 nm with a microplate reader. The viability of cells was determined by the MTT colorimetric assay and results were shown in % of cell viability in comparison with non-treated cells as 100% cell viability [2, 14].

c. *In vitro* cell permeability study:

In vitro cell permeability study was performed to determine permeability of drug across fibroblast monolayer (apical to basolateral). Transwell® inserts of 12 mm diameter, 0.4 µm pore size (Corning, USA) with surface area of 1.12 cm^2 were used. According to standard protocol for permeability study, fibroblast cells were cultivated on filter support at a density of 4×10^5 cells per well. The cells were maintained by changing media every alternate day for 21 days. The integrity of the monolayers was checked by monitoring the trans-epithelial resistance measurement using Millicell® ERS meter (Millipore, Bedford, Massachusetts, USA). After incubation, transepithelial permeation from AP to BL was carried out by placing pure drug and their formulations equivalent to 300 µg prepared in growth medium on the AP side, and 2.5 mL of DMEM on the BL side. Samples (200 µL) were withdrawn from BL compartments at predetermined time interval over 12 hrs. Withdrawn samples were stored at −20 °C until analyzed by HPLC (described in chapter-3). The apparent permeability coefficient (Papp in cm/s) from apical-to-basolateral was calculated as follows:

$$\text{Papp} = \frac{\text{Flux}}{\text{Initial concentration}}$$

…….equation- 5.5.

Where, Papp is the apparent permeability co-efficient (cm/s) and initial concentration applied on the AP side (µg) [34-36].

5.9. Stability study:

The storage stability of drug loaded glycerosomes and liposomes was carried out at different temperatures viz. 2-8°C, 25±2°C/60±5 % RH and 40±2°C/75±5 % RH in air tight container for 90 days. Samples were monitored by analysing for average vesicles size and % assay at interval of 15 days. All parameters were performed in triplicates [5, 25, 37].

5.10. Results and discussion:

ATO loaded glycerosomes: Formulation development

The present research work describes the formulation and evaluation of ATO loaded glycerosomes along with the determination of various critical variables that influence VS and %EE. Following their identification and selection of critical variables, they underwent preliminary analysis to determine their appropriate operating ranges, which were then used to optimise each of the factors using surface response methodology.

5.11. Preliminary screening for ATO loaded glycerosomes:

5.11.1. Risk analysis and mitigation:

Risk analysis is the determination of important factors, the slight change in which can result in decline in product quality. The FishBone diagram (Figure- 5.2) was constructed on the basis of a literature review to identify formulation and process variables that might alter the quality of formulation development of glycerosomes. The quality target or critical quality attributes (CQA) for ATO loaded glycerosomes was maximum entrapment efficiency with minimum vesicle size, as these factors are connected to the therapeutic efficacy of the fabricated glycerosomes. During the preliminary tests, the variables with a low or medium influence on the glycerosomes were optimised using the One Variable At a Time (OVAT) technique, whilst the high-risk factors were taken into consideration and optimised using the definitive screening design (DSD). Only process and formulation factors were examined for risk analysis in this case, whereas drug substance properties were assumed to be constant because the drug utilised was of the same lot number throughout the study.

Table- 5.5. Risk analysis to identify critical parameters for formulation of ATO loaded glycerosomes

Critical Quality Attributes (CQA)	Process variables		Formulation Variables		
	Amplitude of sonication	Sonication cycle	Lipid:drug molar ratio	Cholesterol:drug molar ratio	Glycerol concentration
Vesicle Size (d.nm)	H	H	H	H	H
Entrapment efficiency (%)	H	H	H	H	M

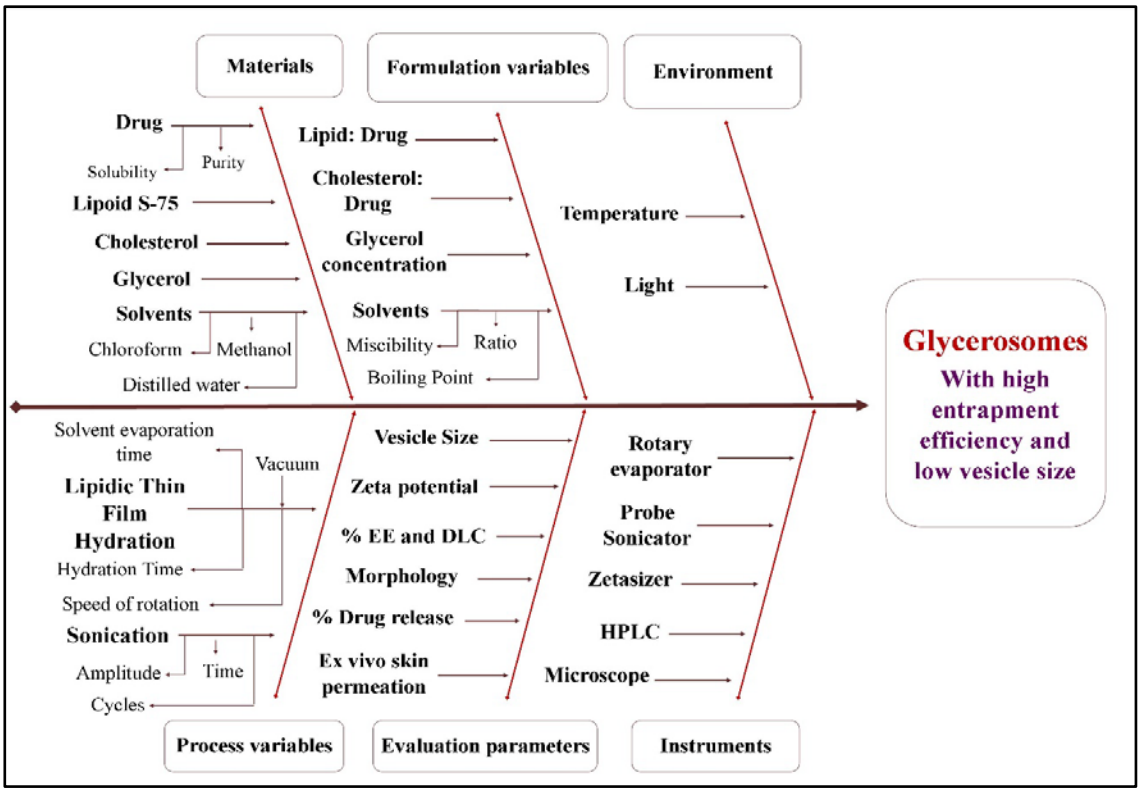

Figure- 5.2. FishBone diagram for selection of variables for development of glycerosomes

5.11.2. Selection of method of preparation and lipid:

Based on trial and error as well as prior research articles, a list of variables that could affect VS and %EE was made. From the numerous factors influencing the quality attributes of glycerosomes, important factors with the greatest and most significant impact on the desired quality attributes of glycerosomes were chosen for preliminary investigation.

An important criterion for the development of glycerosomes is the selection of the best-suited method of preparation. Along with method selection, lipid selection also had a significant impact on vesicle size and entrapment efficiency. Amongst the various reported methods, we attempted thin lipidic film hydration and reverse phase evaporation method. Based on minimum vesicle size and maximum entrapment efficiency, the thin lipidic film hydration method was selected for the preparation of glycerosomes. Amongst the several lipids and their combinations, Lipoid S-75 showed highest entrapment efficiency with minimum vesicle size than other lipids (shown in table- 5.6). Hence, Lipoid S-75 was selected as lipid for preparation of glycerosomes.

Table- 5.6. Selection of method of preparation and lipid

Selection of method of glycerosomes preparation		
Method of preparation	**Observation**	
	Vesicle Size (d.nm)	**Entrapment efficiency (%)**
Lipidic thin film hydration method	288.9 ± 10.2	81.31 ± 2.64
Reverse phase evaporation method	377.8 ± 41.18	65.58 ± 5.56
Selection of lipid		
Lipid and their combination	**Observation**	
	VS (d.nm)	**%EE**
Lipoid S-100	Vesicles visible by naked eyes	
Lipoid S-75	288.9 ± 5.55	82.61 ± 0.90
DPPC	340.6 ± 16.69	78.98 ± 1.90
Phospholipon 90H	358.2 ± 23.10	76.22 ± 2.81
Phospholipon 80H	315.8 ± 10.54	71.86 ± 1.67
Lipoid S-75: DPPC::1:1	298.6 ± 9.56	77.51 ± 3.02

(n=3, ± S.D.)

5.11.3. Screening and optimization of process parameters of lipid film formation:

Process parameters for lipid film formation such as solvents, solvent evaporation temperature and time, vacuum condition, speed of rotation for film formation and hydration, etc. were optimized as per following:

Table- 5.7. Effect of process parameters for formation of lipid film

Selection of organic solvents	
Solvents	**Observation**
Chloroform	Lipid not completely soluble
Chloroform: Methanol (1:1)	Lipid, cholesterol and ATO are completely soluble
Solvent evaporation time (At 60°C, 100 RPM, 400 mmHg)	
Time (min)	**Observation**
15	Inefficient drying, gel like and sticky film
30	Efficient drying
45	Efficient drying
Vacuum condition (30 min at 60°C, 100 RPM)	
Vacuum (mmHg)	**Observation**
200	Inefficient drying, film not properly formed
300	Inefficient drying, film not properly formed
400	Efficient drying with uniform lipid thin film
500	Efficient drying but bubbles were found at bottom of flask.
Speed of rotation for film formation (for 30 minutes at 60°C and 400 mmHg)	
Speed of rotation (RPM)	**Observation**
50	Thin uniform film was not formed.
75	Thin uniform film was not formed.
100	Uniform to irregular film was formed.
125	Uniform to irregular film was formed.
150	Thin uniform film was formed.
175	Thin uniform film was formed.

Speed of rotation for film formation (for 30 minutes at 60°C and 400 mmHg)	
Speed of rotation (RPM)	**Observation**
50	Incomplete hydration, improper removal of film.
75	Incomplete hydration, improper removal of film.
100	Incomplete hydration
125	Incomplete hydration
150	Complete hydration and removal of film completely.

The results of screening of process parameters for lipid thin film formation are shown in table- 5.7. The lipid was completely soluble in chloroform: methanol in ratio of 1:1 ratio, which was selected as solvent system for lipid phase. The presence of residual organic solvent might destabilize the glycerosomes, hence the removal of organic solvent was important process parameter. 30 minute was sufficient to remove organic solvents in rotary evaporator followed by overnight drying in desiccator under reduced pressure. Hence, 30-minute solvent evaporation time was chosen as the optimal duration for solvent evaporation. 400 mmHg vacuum condition selected as optimum due to the formation of proper thin and dry film of lipid. The speed of rotation for thin film formation was affected on the uniformity of lipid film. The effective surface for evaporation during film formation varies with flask rotation speed. At 150 rpm, a thin, uniform, and dry lipidic film was formed; hence, it was chosen as a suitable speed of rotation for thin film formation. For hydration of the film, at 150 rpm, the lipidic film was completely hydrated by the hydration medium and formed a homogenous dispersion of glycerosomes; hence, 150 rpm was selected as the optimum speed of rotation for hydration of the lipid film. The optimum process parameters for formation of lipidic thin film are shown in table- 5.8.

Table- 5.8. Optimized process parameters for lipidic thin film formation

Parameters	Optimum values
Organic phase	Methanol: Chloroform (1:1)
Solvent evaporation time	30 min
Solvent evaporation temperature	60°C
Vacuum condition	400 mmHg
Speed of rotation for film formation	150 rpm
Speed of rotation for film hydration	150 rpm

5.11.4. Screening and optimization of process parameters for preparation of glycerosomes:

Process parameters such as time of hydration, hydration volume, sonication time, sonication amplitude, sonication cycles, etc. were screened and optimized as follows:

a. Selection of time of hydration:

The optimization of the time of hydration was based on visual observation of complete hydration of the lipidic film. Sufficient hydration time was required for the formation of proper vesicle orientation. A shorter hydration time results in inadequate removal of the lipid film, affecting the quality of the glycerosomes. The time of hydration up to 30 min resulted in improper removal of the film and formed a gel like structure at the wall of the flask. At 60 minutes, the lipidic film was completely hydrated. Beyond 60 min, there was no remarkable change (shown in table- 5.9). As a result, 60 min was selected as the optimum hydration time for further development.

b. Selection of hydration volume:

The optimum hydration volume was selected on the basis of visual observation of complete removal of the lipid film. The 5 ml of hydration volume was inadequate to remove the lipid film from the surface of the flask. On 10 ml of hydration volume, the film was completely removed from the surface of the flask and hydrated completely (shown in table-5.9). Thus, 10 ml of hydration medium was considered an optimized volume of hydration for further development.

c. Selection of hydration medium:

Distilled water and phosphate buffer (PBS) pH 7.4 with glycerol were tested for hydration of lipid film. The results showed that, in comparison to PBS pH 7.4, maximum quantity of drug was entrapped in glycerosomes with distilled water as the hydrating medium with a low vesicle size (shown in the table- 5.9). Thus, distilled water containing 20 % w/w glycerol was used as hydrating medium for further development.

d. Selection of pulse of sonication cycle:

As sonication is necessary to convert the micro-sized vesicular dispersion to the nano-sized dispersion, the multilamellar vesicles were subjected to probe sonication for size reduction [38, 39]. The probe sonication parameters showed great impacts on vesicle size and entrapment efficiency. The cycle must be kept in ON-OFF pulse to allow reformation of MLVs to SUVs. During this, the vesicular layer forms which incorporates drug inside the layer. According to the results (shown in the table-5.9), larger vesicles were observed with a 5 sec ON, 5 sec OFF sonication cycle, whereas a 2 sec ON, 2 sec OFF sonication cycle formed vesicles with 361.0 ± 9.16 d.nm VS and 74.58 ± 1.16 % EE. So, for further development, a 2 sec ON, 2 sec OFF pulse of the sonication cycle was selected.

e. Selection of amplitude of sonication:

The amplitude of sonication showed great impact on vesicle size and entrapment efficiency. The results showed that increasing sonication amplitude decreased vesicle size with increasing entrapment efficiency (shown in the table- 5.9), but increasing amplitude beyond 60% leads to increased vesicle size with decreased entrapment efficiency, which could be due to bilayer disruption, which leads to drug expulsion from the lipid bilayer [38, 39]. So, 20-60 % was selected as the sonication amplitude range for further optimization.

f. Selection of sonication cycles:

The number of sonication cycles had a significant impact on vesicle size and entrapment efficiency. The screening of the sonication cycle revealed that as the number of sonication cycles increased, vesicle size decreased and entrapment efficiency increased

(shown in table- 5.9). The 15 -25 sonication cycle was selected for further development as an outcome of the results.

Table- 5.9. Effect of process parameters for preparation of glycerosomes

Time of hydration	
Time (min)	**Observation**
30	Inefficient hydration, not complete removal of film
60	Complete hydration and removal of film with homogenous dispersion of glycerosomes.
75	Complete hydration with homogenous dispersion.

Hydration volume	
Volume (mL)	**Observation**
5	Incomplete removal of film
10	Complete removal of film
15	Complete removal of film

Pulse of sonication Cycles

Pulse of sonication Cycles	**Observations**	
	Vesicle size (d.nm)	**Entrapment efficiency (%)**
5 Sec ON, 5 Sec OFF	Large vesicles were formed which were visible by naked eyes	
2 Sec ON, 2 Sec OFF	361.0 ± 9.16	74.58 ± 1.16

Amplitude of sonication

Amplitude of sonication (%)	**Observations**	
	Vesicle size (d.nm)	**Entrapment efficiency (%)**
10	412.5 ± 9.95	67.12 ± 2.45
20	361.0 ± 6.42	73.18 ± 1.57
40	291.1 ± 9.80	87.77 ± 1.06
60	212.1 ± 8.82	92.60 ± 1.63
70	325.3 ± 10.52	78.60 ± 1.65

Sonication cycles		
Sonication cycles	**Observations**	
	Vesicle size (d.nm)	**Entrapment efficiency (%)**
10	347.7 ± 8.30	73.83 ± 2.36
15	290.8 ± 5.08	80.55 ± 2.98
20	212.1 ± 8.81	88.60 ± 2.06
25	167.3 ± 6.12	93.81 ± 1.85
30	198.2 ± 7.25	82.55 ± 1.63
Hydration medium		
Glycerol containing medium	**Observation**	
	Vesicle size (d.nm)	**Entrapment efficiency (%)**
Distilled water	278.6 ± 5.40	82.61 ± 1.84
PBS pH 7.4	266.9 ± 7.49	76.59 ± 1.69

(n=3, ± S.D.)

After preliminary studies, the optimised process variables for preparation of glycerosomes which were kept constant are shown in table-5.10. Using a design of experiment technique, the high-risk parameters were optimised while keeping these variables constant.

Table- 5.10. Constant process variables for preparation of glycerosomes

Parameters	Optimum values
Time of hydration	60 min
Hydration volume	10 mL
Pulse of sonication cycle	2 sec ON, 2 sec OFF
Hydration medium	Distilled water

5.11.5. Screening and optimization of formulation parameters for glycerosomes preparation:

The screening and optimization of formulation parameters such as lipid:drug molar ratio, cholesterol:drug molar ratio and glycerol concentration are as follows:

Table- 5.11. Effect of formulation parameters on preparation of ATO loaded glycerosomes

Screening of lipid:drug molar ratio		
Lipid:drug molar ratio	**Observations**	
	VS (d.nm)	**% EE**
2:1	146.5 ± 4.72	64.45 ± 2.63
3:1	239.4 ± 5.87	82.61 ± 0.90
4:1	288.9 ± 9.99	87.57 ± 2.45
6:1	338.9 ± 7.45	79.79 ± 1.33
8:1	412.2 ± 14.36	71.05 ± 2.78
Screening of cholesterol:drug molar ratio		
Cholesterol:drug molar ratio	**Observations**	
	VS (d.nm)	**% EE**
0:1	255.9 ± 7.63	70.57 ± 1.62
0.25:1	311.8 ± 9.41	74.34 ± 2.73
0.5:1	337.1 ± 9.80	80.16 ± 1.27
1:1	287.2 ± 5.15	89.03 ± 0.93
1.5:1	435.9 ± 18.48	85.36 ± 1.59
Screening of glycerol concentration		
Glycerol concentration (%)	**Observations**	
	VS (d.nm)	**% EE**
0	204.3 ± 5.41	81.08 ± 1.80
10	268.5 ± 7.33	86.36 ± 1.05
20	290.5 ± 9.80	90.12 ± 2.48
30	304.6 ± 5.26	88.22 ± 1.05
40	552.1 ± 20.47	80.38 ± 1.57

(n=3, ± S.D.)

a. Screening of lipid:drug molar ratio:

In vesicular drug delivery systems, lipid is an important component for bilayer formation. The results showed that, increase in lipid moles increases vesicle size and entrapment efficiency upto 4:1 of lipid:drug molar ratio. When the lipid:drug molar ratio

is increased beyond a 4:1, the entrapment efficiency of the drug can decrease. This is because at high lipid:drug molar ratio, the lipids can form aggregates or clusters, which can lead to a reduction in the available space for drug encapsulation. Also, the drug molecules may not be able to effectively partition into the interior of the lipid bilayer and become unentrapped, leading to a lower entrapment efficiency [40, 41]. Hence, 2:1 to 6:1 mole ratio of lipid with drug were selected for further development.

b. Screening of cholesterol:drug molar ratio:

Cholesterol does not form a bilayer, but it is dispersed in a lipidic bilayer, which increases the fluidity and stability of the bilayer. Cholesterol concentration had a significant impact on the vesicle size and entrapment of drug in vesicles. The effect of increasing the cholesterol mole ratio showed an increase in entrapment efficiency up to a 1:1 ratio; however, increasing the cholesterol:drug mole ratio up to a 1.5:1 ratio increased vesicle size and decreased entrapment efficiency, which could be due to the fact that at a higher concentration, cholesterol hardens the bilayer, making incorporation of drug molecule harder, resulting in a decrease in EE. Hence, 0:1 to 1:1 cholesterol mole ratio with drug was selected for further optimization.

c. Screening of glycerol concentration:

From the results of screening study, it was found that increase in concentration of glycerol increases vesicle size and entrapment efficiency upto certain level (20% w/w glycerol concentration), after which that EE was decreased with increase in glycerol concentration. At 20 % w/w glycerol concentration, the vesicle size was found to be 290.5 ± 9.80 d.nm with 90.12 ± 2.48 % EE. Beyond that, upto 30% glycerol concentration, there was no remarkable difference observed in VS as well as % EE. With the further increase in glycerol concentration up to 40% w/w, there was a slight decrease in the % EE, which might be due to an increase in the viscosity of the intervesicle medium, which hindered the reduction of vesicle size and subsequently decreased the surface area for drug encapsulation [42, 43]. Hence, 20 % w/w glycerol concentration was selected for further development.

Using a design of experiment technique, the high-risk parameters were optimised while keeping other process and formulation variables constant.

5.12. Design of experiment: Definitive screening design for optimization of glycerosomes

The effect of different process and formulation parameters on quality of product was analyzed by using Definitive Screening Design (DSD). The influence of four factors at three levels was studied with the novel design, termed as Definitive Screening Design (DSD). The variables evaluated for formulation were lipid:drug mole ratio, cholesterol:drug mole ratio, amplitude for sonication and cycles of sonication.

5.12.1. Design matrix

DesignExpert software generated a randomised matrix of thirteen batches, as shown in table-5.12.

Table- 5.12. Experimental runs and their results for ATO loaded glycerosomes

Run	Factor A	Factor B	Factor C	Factor D	Response 1	Response 2
	Lipid:drug molar ratio	Cholesterol: drug molar ratio	Amplitude	Sonication cycle	VS	EE
					d.nm	%
A1	6:1	0.5:1	20	25	253.1 ± 5.61	76.66 ± 1.52
A2	4:1	0.5:1	40	20	207.8 ± 7.03	84.54 ± 1.69
A3	6:1	0:1	60	25	203.2 ± 8.63	80.77 ± 2.31
A4	6:1	1:1	60	15	245.8 ± 5.12	75.57 ± 0.98
A5	2:1	1:1	40	25	158.1 ± 2.69	68.54 ± 2.12
A6	2:1	0.5:1	60	15	169.0 ± 4.21	64.18 ± 1.23
A7	4:1	0:1	20	15	181.8 ± 3.98	76.98 ± 1.58
A8	2:1	1:1	20	15	188.9 ± 5.12	57.67 ± 2.63
A9	6:1	0:1	40	15	252.6 ± 9.65	72.45 ± 2.12
A10	2:1	0:1	60	20	159.3 ± 3.41	66.15 ± 2.01
A11	2:1	0:1	20	25	162.2 ± 2.33	61.14 ± 1.26
A12	6:1	1:1	20	20	294.1 ± 6.98	75.54 ± 5.22
A13	4:1	1:1	60	25	155.5 ± 2.18	90.38 ± 1.36

(n=3, ± S.D.)

The effect of independent variables on responses are discussed below:

5.13. Effect of independent variables on vesicle size:

The values of vesicle size varied from 155.5 to 294.1 d.nm throughout all 13 runs due to variation in independent factor combinations. From the statistical analysis, we can observe that R^2 value for actual Vs predicted values for vesicle size was 0.9768 which is good correlation.

ANOVA results of model:

Summary of the ANOVA results of different models for vesicle size is shown in table- 5.13 which depicts model p-value with adjusted and predicted R^2 values.

Table- 5.13. Summary of ANOVA results of different models for vesicle size

Source	Model p-value	Adjusted R^2	Predicted R^2	
Design Model	**0.0006**	**0.9768**	**0.9152**	**Recommended**
Linear	0.0026	0.7658	0.5947	Suggested
2FI	0.0268	0.9746	0.8094	**Aliased**

The polynomial with lowest p-value ($p<0.05$) was considered for model selection (shown in table- 5.13). Based on the results obtained from the experiments and criteria, design model was recommended to be best fitted to the observed responses. Other models were not suitable for prediction either due to low R^2 value or due to high p value as compared to design model [44].

ANOVA results of design model for vesicle size as shown in 5.14 revealed that the effect of factors was significant and hence the model was significant for the vesicle size. The Model F-value of 64.11 implies the model was significant. There was only a 0.06% chance that an F-value this large could occur due to noise. The p-values less than 0.05 indicate model terms are significant. In this case A, B, C, D, A^2, D^2 were significant model terms. Values greater than 0.10 indicate the model terms are not significant. The F value of factor A was highest (352.99) i.e., maximum effect on vesicle size, while factors B, C and D had low effect on vesicle size on the basis of F value.

Table- 5.14. ANOVA results of design model for vesicle size

Source	Sum of Squares	df	Mean Square	F-value	p-value	
Model	24579.00	8	3072.38	64.11	0.0006	**Significant**
A-Lipid:drug molar ratio	16916.77	1	16916.77	352.99	< 0.0001	
B-Cholesterol:drug molar ratio	693.89	1	693.89	14.48	0.0190	
C-Amplitude	2169.73	1	2169.73	45.27	0.0025	
D-Sonication cycle	1123.60	1	1123.60	23.45	0.0084	
A^2	2305.88	1	2305.88	48.12	0.0023	
B^2	225.60	1	225.60	4.71	0.0958	
C^2	42.84	1	42.84	0.8940	0.3979	
D^2	1465.99	1	1465.99	30.59	0.0052	
Residual	191.70	4	47.92			
Cor Total	24770.70	12				

Table- 5.15. Summary of ANOVA results for vesicle size

Parameters	Results	Parameters	Results
Std. Dev.	6.92	**R^2**	0.9923
Mean	202.42	**Adjusted R^2**	0.9768
C.V. %	3.42	**Predicted R^2**	0.9152
		Adeq. Precision	24.1734

The predicted R^2 of 0.9152 is in reasonable agreement with the Adjusted R^2 of 0.9768; i.e., the difference is less than 0.2 (shown in table- 5.15). The Adeq. Precision measures the signal to noise ratio and ratio greater than 4 is desirable. The ratio of 24.173 indicates an adequate signal. This model can be used to navigate the design space.

Model diagnostic plots:

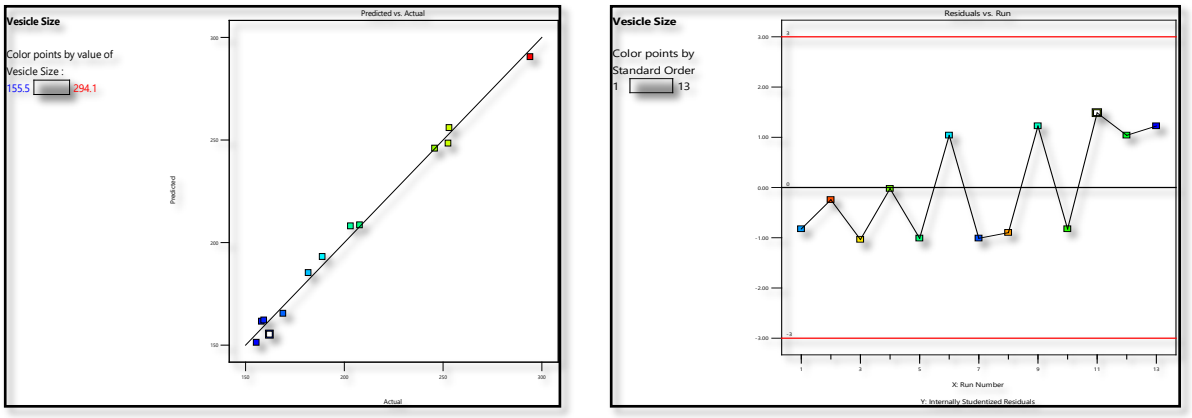

a. Predicted Vs actual

b. Residual vs run

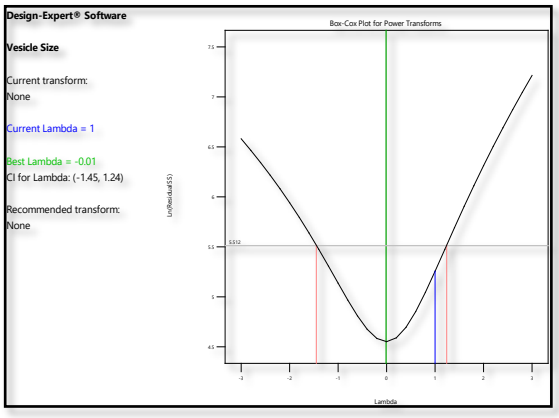

c. Box-Cox plot for power transforms

Figure – 5.3. Model diagnostic plots for vesicle size

a. Plot of Predicted Vs actual
b. Plot of Residual vs run
c. Box-Cox plot for power transforms

For evaluation of model, various diagnostic plots are shown in figure- 5.3. The **predicted Vs actual plot** (figure- 5.3a) depicts correlation between the observed and actual response values. The good correlation between observed and predicted values shows that the model chosen for analysis of variance is appropriate to predict the responses all over the design matrix. This plot will help to detect values that are not easily predicted by the model. The predicted Vs actual plot (shown in figure-5.3a) follows a 45° straight line indicating a close estimation of predicted values with actual values.

Figure- 5.3b represents graph of **residuals vs the order of the experimental runs**. It looks for hidden factors that might have impacted the experiment's outcome. The scatter should be random on the plot [45]. The residual versus run plot (figure- 5.3b) indicates a random distribution of residuals in the current study, indicating the absence of hidden variables.

The **plot of Box-Cox for power transformation** (figure- 5.3c) serves as a reference for choosing the appropriate power law transformation. Based on the best lambda value determined at the lowest point of the curve created by the natural log of the sum of squares of the residuals, a proposed transformation is given. If the 95% confidence interval around this lambda contains 1, the software does not propose a specific transformation. When the logit or arcsine square root transformations are used, this plot is not utilised [45]. The plot of power transformation (figure- c) shows the λ value of 1, which lies near to the best λ value and within 95% confidence interval of it, indicating no requirement for any power transformation.

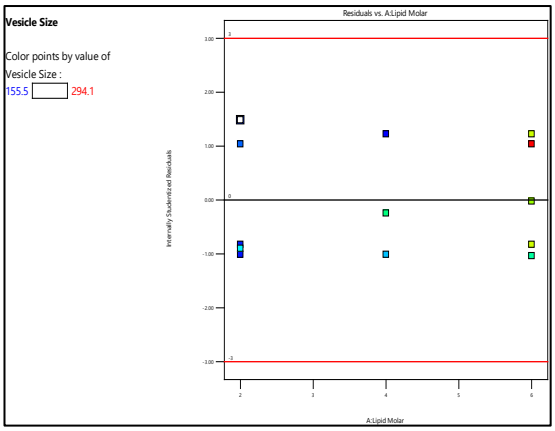

a. Residual Vs Lipid:drug molar ratio

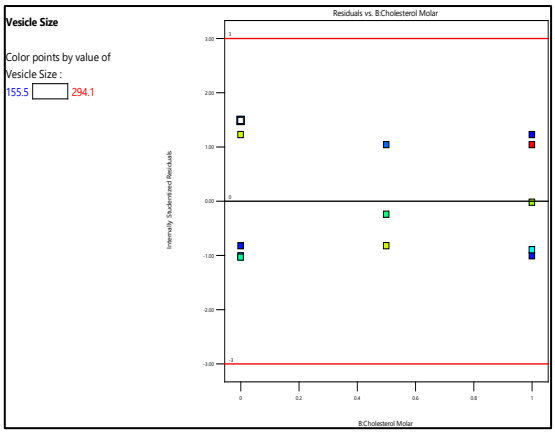

b. Residual Vs Cholesterol:drug molar ratio

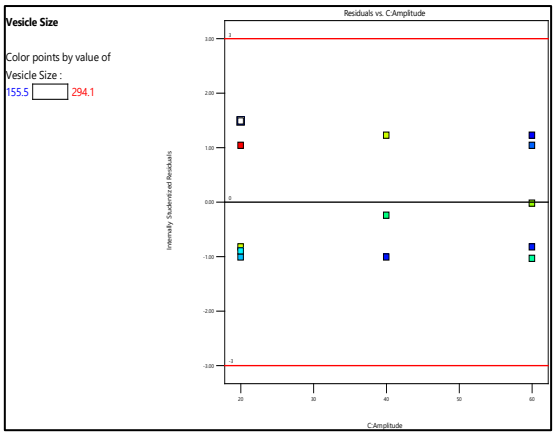

c. Residual Vs Amplitude

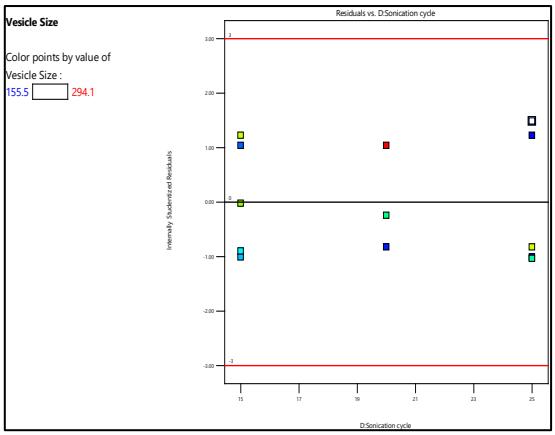

d. Residual Vs Sonication cycle

Figure- 5.4. Residual Vs factor plots

a. Residual Vs Lipid:drug molar ratio
b. Residual Vs Cholesterol:drug molar ratio
c. Residual Vs Amplitude
d. Residual Vs Sonication cycle

Figure- 5.4 represents graph of the **residuals vs whatever factor** selected for optimization. It evaluates if the variable not accounted for by the model varies with the level of a factor. If everything is in order, the plot should show a random dispersion. Pronounced curvature may suggest a systematic contribution of the independent factor that the model does not compensate for. The residual versus factor plot reveals if there is a correlation between the variance associated with different levels of factor, i.e., any distinctive trends (+ve or -ve curvature) correlated with increasing levels of each factor [45]. The plots for each factor, as shown in the figure-5.4, show a random scattering throughout the levels of factor, demonstrating that the model is effective in accounting for the variation for each variable.

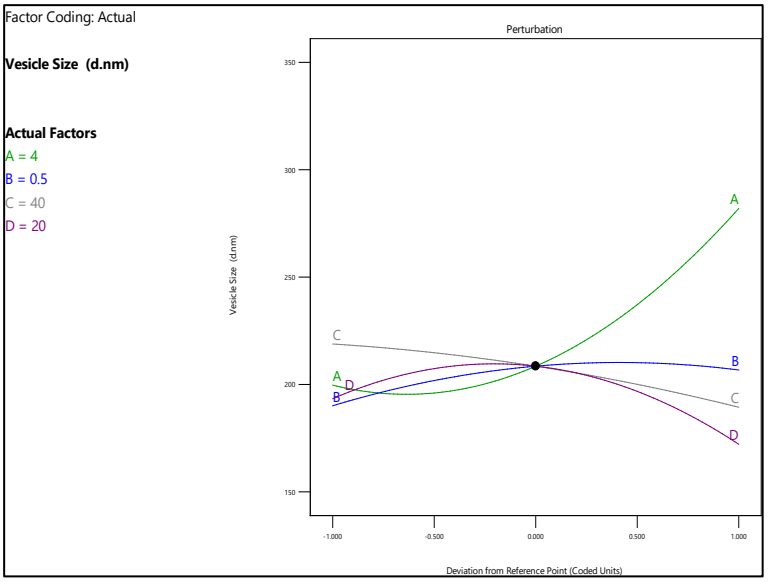

Figure – 5.5. Pipel's plot on response variable 1 (Vesicle size)

Pipel's plot is a trace plot showing the effect of individual factors by plotting the pseudo-limits of one component while keeping the other constant against the response. The responses are plotted as deviations from the reference blend i.e., centroids (Pseudo centre point of the constrained design). As it can be seen from the plot (shown in figure- 5.5), lipid:drug molar

ratio showed positive effects on the vesicle size indicated by increase in the vesicle size along with the increase in the lipid:drug molar ratio.

Model plots: Response surface plot (3D plot):

The value of ANOVA gives us idea about the factors having significant effect on vesicle size which is shown in 3D plots (figure-5.6). The red region in this graph represents the maximum vesicle size, while the blue area represents the smallest vesicle size.

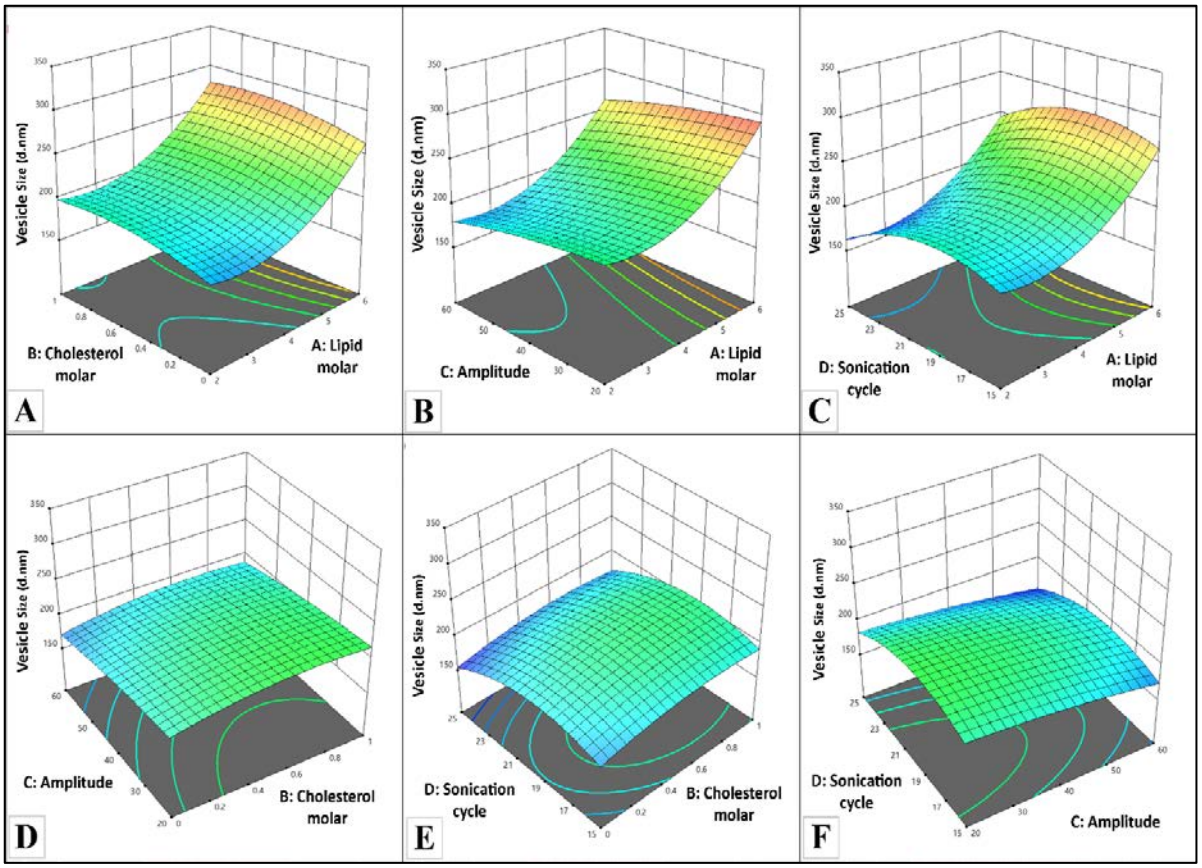

Figure- 5.6. Response surface plot (3D) showing combined effect of independent variables on vesicle size

(A)- Combined effect of Lipid:drug molar ratio and Cholesterol:drug molar ratio

(B)- Combined effect of Lipid:drug molar ratio and Amplitude

(C)- Combined effect of Sonication cycle and Lipid:drug molar ratio

(D)- Combined effect of Amplitude and Cholesterol:drug molar ratio

(E)- Combined effect of Sonication cycle and Cholesterol:drug molar ratio

(F)- Combined effect of Sonication cycle and Amplitude

Response surface plot (3D) showing combined effect of independent variables on vesicle size is shown in figure- 5.6. The magnitude of factor A (equation-5.5) showed positive effects on vesicle size, denoting an increase in vesicle size with an increase in the lipid:drug molar ratio. The magnitude of factor B (equation-5.5) showed positive effects on vesicle size, which represented an increase in vesicle size with an increase in the cholesterol mole ratio. The amplitude of factor C (equation-5.5) showed negative effects on vesicle size, indicating that an increase in the amplitude of sonication decreased the vesicle size. The amplitude of factor D (equation-5.5) denoted the negative effects on vesicle size; hence, an increase in the number of sonication cycles decreases the vesicle size.

From the 3D surface plot and polynomial equation (equation-5.5), it was found that an increase in vesicle size is associated with an increase in the lipid:drug as well as cholesterol:drug molar ratio. The increase in vesicle size with increase in cholesterol:drug molar ratio could be imputed to the increased rigidity of vesicle membrane. Hence, vesicle size is increased in an endeavour to achieve thermodynamic stability [1, 46]. In addition, the increased vesicle size with increasing cholesterol:drug molar ratio might be due to enhanced vesicle membrane rigidity, which could result in resistance to size reduction during the sonication stage [47]. The increase in amplitude of sonication and number of sonication cycles decrease the vesicle size. The decrease in the vesicle size becomes faster by increasing the amplitude and number of sonication cycles as is expected due to conversion of large lamellar vesicles to small bilayer vesicles [48]. It occurred due to the lipid molecules of vesicles might rearrange and reassemble to form smaller vesicles under suitable probe-sonication condition [7, 49].

Polynomial equation for vesicle size:

The polynomial equations were obtained from design for vesicle size are as follows:

Final equation in terms of coded factors:

$$\text{Vesicle size (d.nm)} = + 208.54 + 41.13 * A + 8.33 * B - 14.73 * C - 10.60 * D + 32.30 * A^2 - 10.10 * B^2 - 4.40 * C^2 - 25.75 * D^2$$

……equation- 5.5.

Reduced equation in terms of coded factors:

$$\text{Vesicle size (d.nm)} = + 208.54 + 41.13 * A + 8.33 * B – 14.73 * C - 10.60 * D + 32.30 * A^2 - 25.75 * D^2$$

……equation- 5.6.

5.14. Effect of independent variables on % EE:

The values of entrapment efficiency varied from 57 to 90 % throughout all 13 runs due to variation in independent factor combinations. From the statistical analysis, we can observe that R^2 value for actual Vs predicted values for % EE was 0.9849 which is good correlation.

ANOVA results of model:

Summary of the ANOVA results of different models for % EE is shown in table-5.16 which depicts model p-value with adjusted and predicted R^2 values.

Table- 5.16. Summary of ANOVA results of different models for % EE

Source	Model p-value	Adjusted R^2	Predicted R^2	
Design Model	**0.0003**	**0.9847**	**0.9368**	**Recommended**
Linear	0.1242	0.3356	-0.0456	Suggested
2FI	0.4205	0.4633	0.3672	Aliased

The polynomial which showed the lowest p values (<0.05) was considered for model selection. On the basis of criteria, the design model was found to be best fitted to the observed responses and chosen for further evaluation.

Table- 5.17. ANOVA results of design model for % EE

Source	Sum of Squares	df	Mean Square	F-value	p-value	
Model	1052.89	8	131.61	97.43	0.0003	**Significant**
A-Lipid:drug molar ratio	400.82	1	400.82	296.72	< 0.0001	
B-Cholesterol:drug molar ratio	10.42	1	10.42	7.72	0.0499	
C-Amplitude	84.45	1	84.45	62.52	0.0014	
D-Sonication cycle	93.88	1	93.88	69.50	0.0011	
A^2	421.71	1	421.71	312.19	< 0.0001	
B^2	0.6739	1	0.6739	0.4989	0.5190	
C^2	0.8694	1	0.8694	0.6436	0.4674	
D^2	2.11	1	2.11	1.56	0.2794	
Residual	5.40	4	1.35			
Cor Total	1058.29	12				

ANOVA results of design model for % EE is shown in table- 5.17 revealed that independent factors significantly influenced responses, and hence the model shows significance for EE. The model F-value of 97.43 implies the model is significant. There is only a 0.03 % chance that an F-value this large could occur due to noise. The p-values less than 0.0500 indicate model terms are significant. In this case, A, B, C, D, A^2 are significant model terms. Values greater than 0.1000 indicate the model terms are not significant.

Table- 5.18. Summary of ANOVA results for % EE

Parameters	Values	Parameters	Values
Std. Dev.	1.16	**R^2**	0.9949
Mean	73.12	**Adjusted R^2**	0.9847
C.V. %	1.59	**Predicted R^2**	0.9368
		Adeq Precision	33.17

The predicted R^2 of 0.9368 is in reasonable agreement with the adjusted R^2 of 0.9847; i.e., the difference was less than 0.2 (shown in table- 5.18). Adeq precision measures the signal-to-noise ratio, which was found to be 33.17, indicating an adequate signal (the ratio must be more than 4). This model can be used to navigate the design space.

Model diagnostic plot:

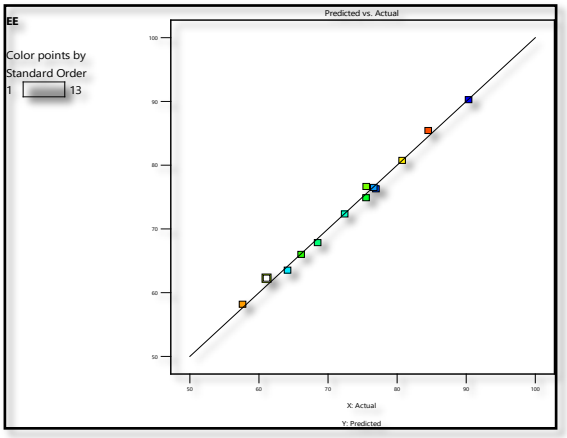

a. Predicted Vs actual

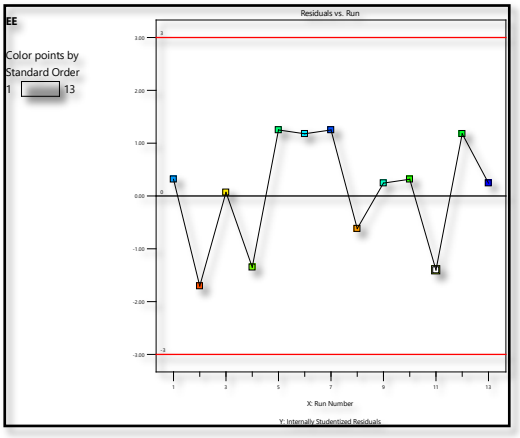

b. Residual vs run

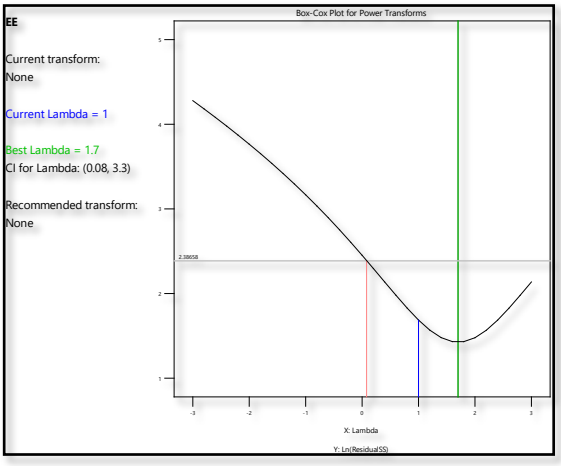

c. Box-Cox plot for power transforms

Figure- 5.7. Model diagnostic plots for % EE

a. Plot of Predicted Vs actual
b. Plot of Residual vs run
c. Box-Cox plot for power transforms

Various diagnostic plots for evaluation of model are shown in figure- 5.7. The predicted vs actual plot (figure- 5.7a) follows a 45° straight line which indicates a close estimation of

actual values with predicted values. The residual vs run plot (figure- 5.7b) shows random distribution of residuals in the current analysis indicated that there was absence of any lurking variable. The Box-Cox plot for power transformation (figure- 5.7c) showed that the λ value of 1, which lies nearer to the best λ values and found within 95% CI of it, indicated that there was no required power transformation.

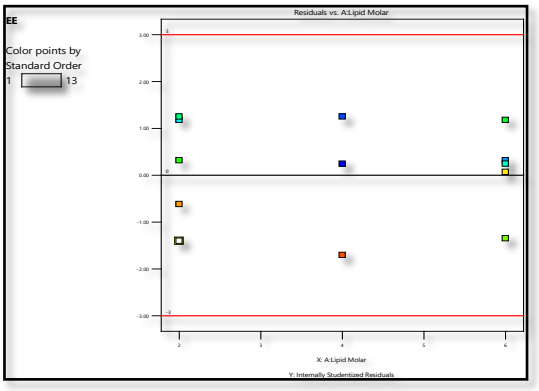

a. Residuals Vs Lipid:drug molar ratio

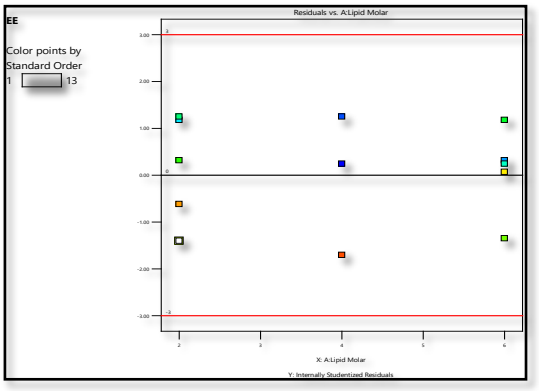

b. Residuals Vs Cholesterol:drug molar ratio

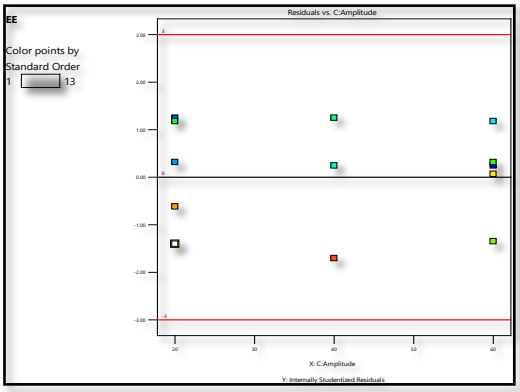

c. Residuals Vs Amplitude

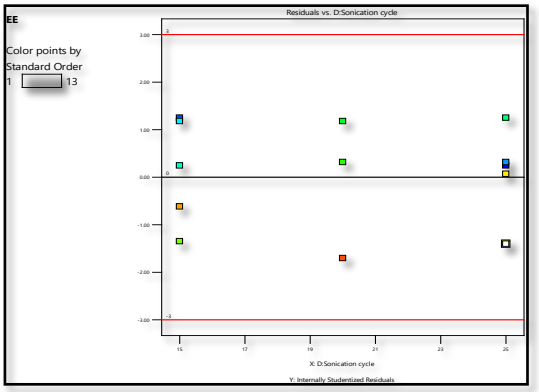

d. Residuals Vs Sonication cycle

Figure- 5.8. Residuals Vs factor plots for % EE

a. Residual Vs Lipid:drug molar ratio
b. Residual Vs Cholesterol:drug molar ratio
c. Residual Vs Amplitude
d. Residual Vs Sonication cycle

The plots for residuals with each factor (shown in figure-5.8) represents a random scattering over increasing levels of factors indicating that the model is effective in accounting for the variance for each factor.

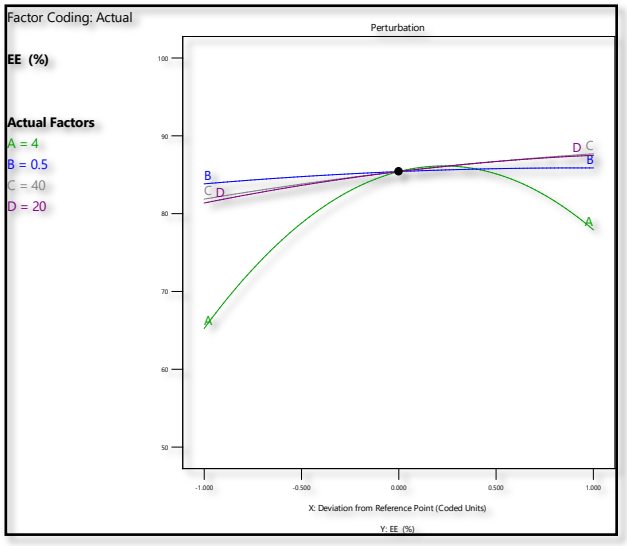

Figure- 5.9. Pipel's plot on response of % EE

The Pipel's plot on the response of % EE (figure-5.9) showed that increased amplitude of sonication increases entrapment efficiency, which indicated a positive effect.

Model Plots: Response surface plot (3D)

The ANOVA data indicate which variables have a significant influence on entrapment efficiency, as seen in the response surface 3D plot (shown in figure-5.10).

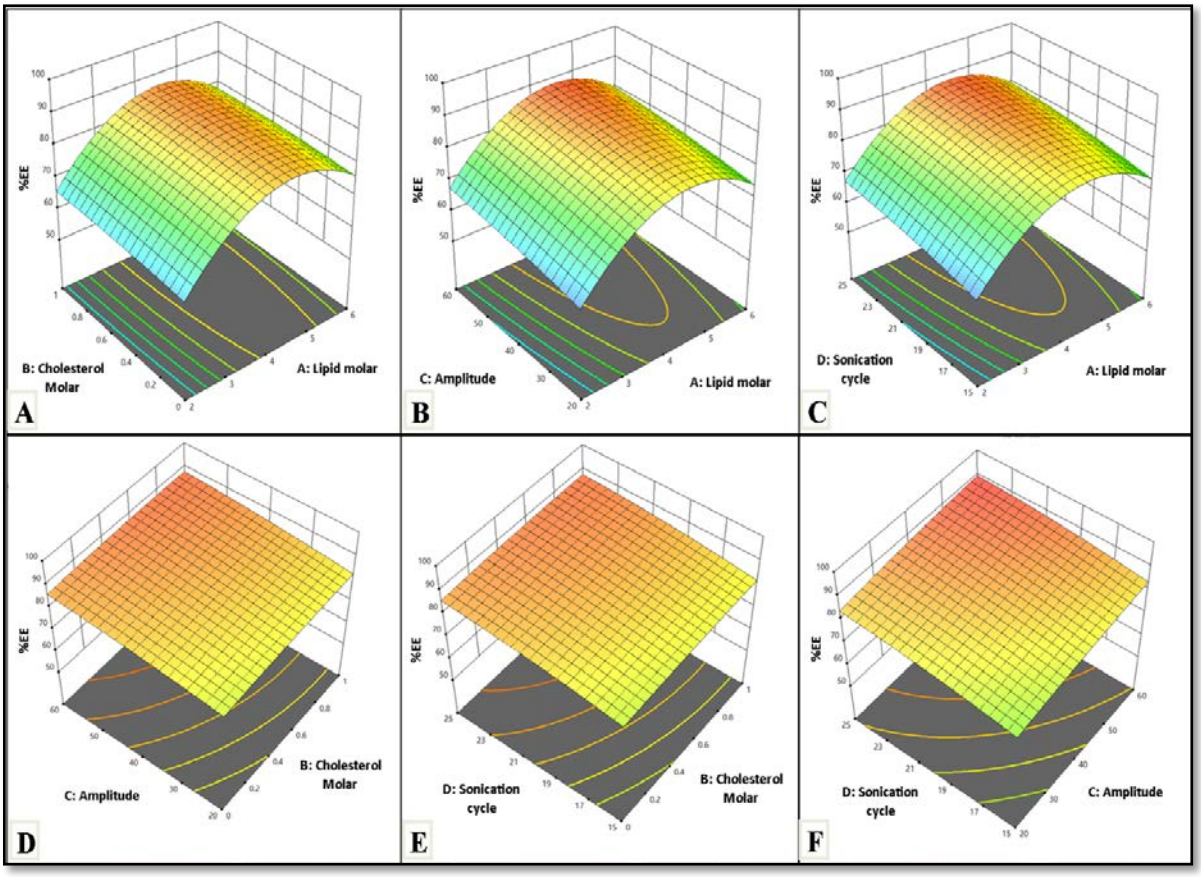

Figure- 5.10. Response surface plot (3D) showing combined effect of independent variables on % EE,

(A)- Combined effect of Lipid:drug molar ratio and Cholesterol:drug molar ratio

(B)- Combined effect of Lipid:drug molar ratio and Amplitude

(C)- Combined effect of Sonication cycle and Lipid:drug molar ratio

(D)- Combined effect of Amplitude and Cholesterol:drug molar ratio

(E)- Combined effect of Sonication cycle and Cholesterol:drug molar ratio

(F)- Combined effect of Sonication cycle and Amplitude

The figure- 5.10 (A-F) represents surface 3D response plot of effect of various variables on % entrapment efficiency. The magnitude of Factor A, Factor B, Factor C, and factor D (equation-5.7) showed positive effect on % EE. It was observed that the increase in lipid:drug ratio increases % EE due to higher surface area available for entrapment due to lipophilic nature of drug [7, 50]. The increase in lipid:drug ratio improved affinity and deposition of atorvastatin into the lipid bilayer of vesicles, leading to high entrapment efficiency [51-53]. The EE increased as the lipid:drug molar ratio increased because glycerosomes could provide sufficient lipid bilayers to accommodate drug molecules, hence accelerating the drug loading process and resulting in high EE [39]. Increased sonication amplitude and cycles led to the

formation of small-sized vesicles, which increased the overall hydrophobic space in the lipid bilayer, which allowed additional space for the drug to reside in, leading to higher EE [7, 54].

Polynomial equation for % EE:

The polynomial equations were obtained from design for entrapment efficiency are as follows:

Final equation in terms of coded factors:

$$\text{Entrapment Efficiency (\%)} = +85.40 + 6.33 * A + 1.02 * B + 2.91 * C + 3.06 * D - 13.81 * A^2 - 0.5521 * B^2 - 0.6271 * C^2 - 0.9771 * D^2$$

…….equation- 5.7.

Reduced equation in terms of coded factors:

$$\text{Entrapment Efficiency (\%)} = +85.40 + 6.33 * A + 1.02 * B + 2.91 * C + 3.06 * D - 13.81 * A^2$$

…….equation- 5.8.

5.15. Desirability plot and overlay plot for optimization:

A desirability plot suggests the optimal values for each variable to get the desired results. The table-5.19 shows the desirable batch parameters.

Table- 5.19. Variables for desirability plot and goals for response

Variables	Goal	Lower limit	Upper limit
A: Lipid:drug molar ratio	In range	2:1	6:1
B: Cholesterol:drug molar ratio	In range	0:1	1:1
C: Amplitude	In range	20	60
D: Sonication cycle	In range	15	25
Vesicle Size (d.nm)	Minimize	155.5	294.1
Entrapment Efficiency (%)	Maximize	57.67	90.38

Desirability criteria and a desirability plot were developed in order to carry out optimization using mathematical function. For this, higher and lower desired response values were chosen, and software created variable values to help produce the desired response. The ramp graph (Figure-5.11c) shows the projected values of R1 and R2 for the optimal concentration of independent variables, while the bar graph (Figure-5.11b) shows individual desired for R1 and R2. The projected answer has a composite desirability of 0.996 (shown in figure- 5.11c).

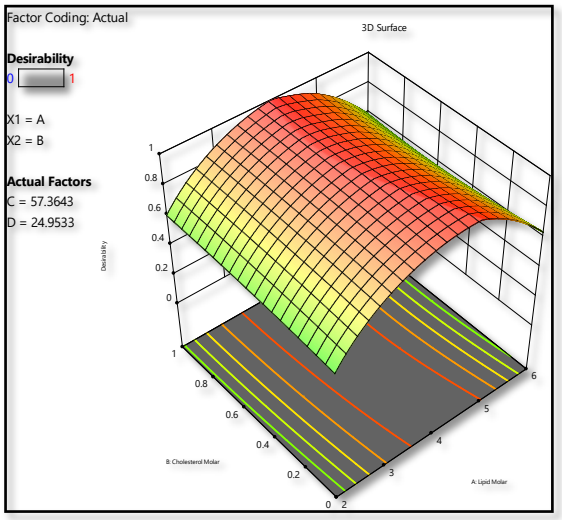

a. 3D Desirability plot

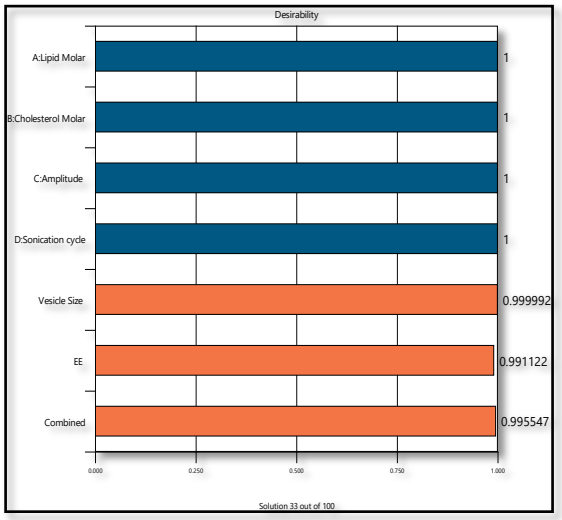

b. Bar graph of desirability

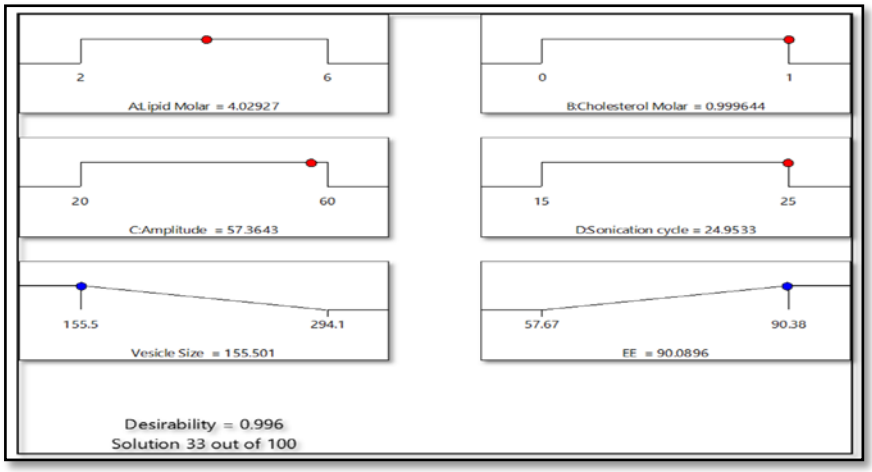

c. Ramp graph of desirability

Figure- 5.11. Desirability plot for ATO loaded glycerosomes

a. 3D Desirability plot

b. Bar graph of desirability

c. Ramp graph of desirability

To evaluate the desirability, ATO loaded glycerosomes formulation was prepared according to the suggested batch, and the obtained response values were determined to be similar with the predicted responses. Furthermore, the design's error was determined to be less than 5%, indicating its eligibility for prediction. This demonstrates that the software-predicted optimum formulation is reliable for practical purposes.

Table – 5.20. Predicted and observed responses of optimized ATO loaded glycerosomes

Variables	Values	Responses	Predicted values	Observed values	% Error
Lipid:drug molar ratio	4.03:1	**VS (d.nm)**	155.5	159.75 ± 5.82	2.73
Cholesterol :drug molar ratio	0.99:1	**EE (%)**	90.08	88.81 ± 2.33	1.41
Amplitude	57.36				
Cycles of sonication	24.95				

(n=3, ± S.D.)

The obtained observed values (in table-5.20) were nearly related to the predicted values obtained from check point batch which is acceptable with % error. The predicted and observed values do not differ significantly at $p \leq 0.05$, hence, the results ensure the reliability of the optimization procedure.

5.16. Graphical optimization to generate control space:

For both vesicle size and % EE, it is essential to select an area that offers the best value of variables. Overlay plots may be generated by superimposing counter plots of both responses in the factor space, which displaces the region of feasible response values. The region of yellow is the area where a little variation in the critical variables has no influence on the final answer and the response falls within the desired range. The grayed-out area does not comply with the optimization criteria. This approach strengthens the design by narrowing the design space and providing tolerance interval of alpha level of 0.05 to the responses. The overlay plot of design is shown in figure-5.12.

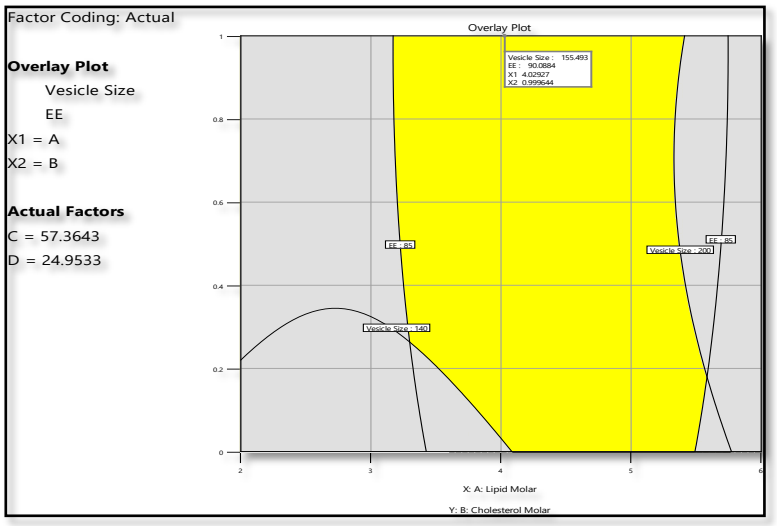

Figure- 5.12. Overlay plot for design space

5.17. Analysis of design space:

Evaluating the design space for robustness is essential. This provides insight into the result's repeatability when formulation development is carried out in that specific design area. Three formulations were picked at random from the plotted design space to analyse the robustness of design space. The formulation was prepared using the provided values for the factors, and the predicted and observed values of the responses were compared.

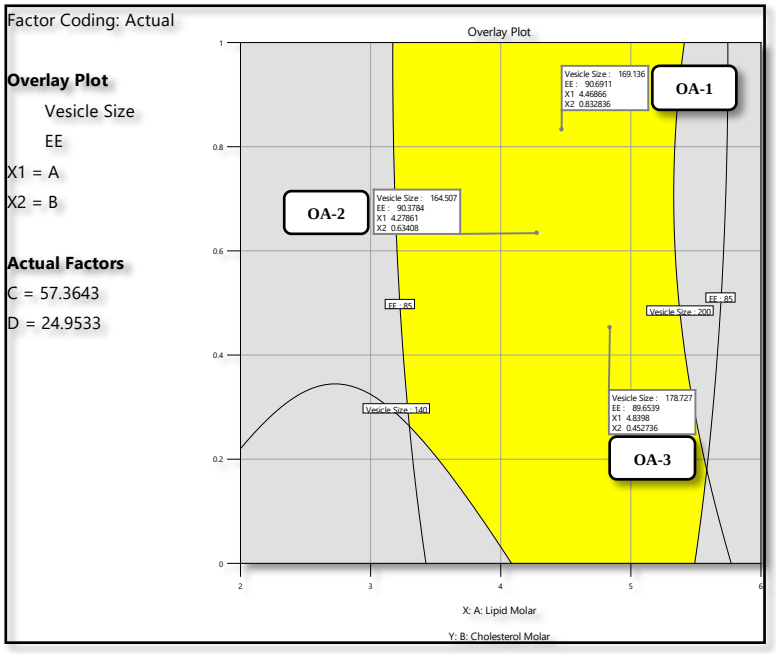

Figure- 5.13. Analysis of design space

Table- 5.21. Check point batch analysis

Formulations	Parameters	Predicted	Observed	Std. Error
OA-1	**VS (d.nm)**	169.13	165.77 ± 4.93	1.98
	% EE	90.69	86.79 ± 1.86	3.19
OA-2	**VS (d.nm)**	164.50	166.23 ± 3.59	1.05
	% EE	90.37	87.92 ± 1.11	2.71
OA-3	**VS (d.nm)**	178.72	171.03 ± 4.24	3.74
	% EE	89.65	87.74 ± 1.49	2.13

(n=3, ± S.D.)

According to the robustness analysis, the observed responses remained within the boundary, and the variation between predicted and observed values was not significant.

5.18. Point prediction and confirmation:

The predicted responses for the optimized batch selected from design space are shown in table-5.22. The optimized values of responses were confirmed by carrying out the experiment using

the selected factor values in triplicate. On the basis of the results (table-5.20), it was confirmed that the observed values were found to be nearer to predicted values, concluding that the selected model for optimization was suitable.

Table – 5.22. Predicted responses for selected solution along with standard deviation

Response	Predicted Mean (d.nm)	Observed mean (d.nm)	Std Dev	SE Pred	95% PI low	95% PI high
VS	155.50	159.75 ± 5.82	6.92	7.00	136.06	174.93
%EE	90.08	88.81 ± 2.33	1.16	1.18	86.82	93.35

(n=3, ± S.D.)

5.19. Physicochemical characterization of optimized batch:

5.19.1. Vesicle size, PDI and zeta potential determination:

The glycerosomes must have nanosized mean vesicle size with a narrow size distribution, a biocompatible zeta potential, and efficient drug loading to have therapeutic promise as a drug delivery system. Vesicle size is an important parameter, as it can have an influence on drug release properties and the permeation of drugs through the skin. The average vesicle size, polydispersity index and zeta potential of optimized batch as measured by zetasizer was found to be 159.75 ± 5.82 d.nm, 0.350 ± 0.106 and -6.08 ± 0.66 mV respectively. The negatively charged vesicular formulations can strongly improve skin permeation in transdermal delivery [8, 55].

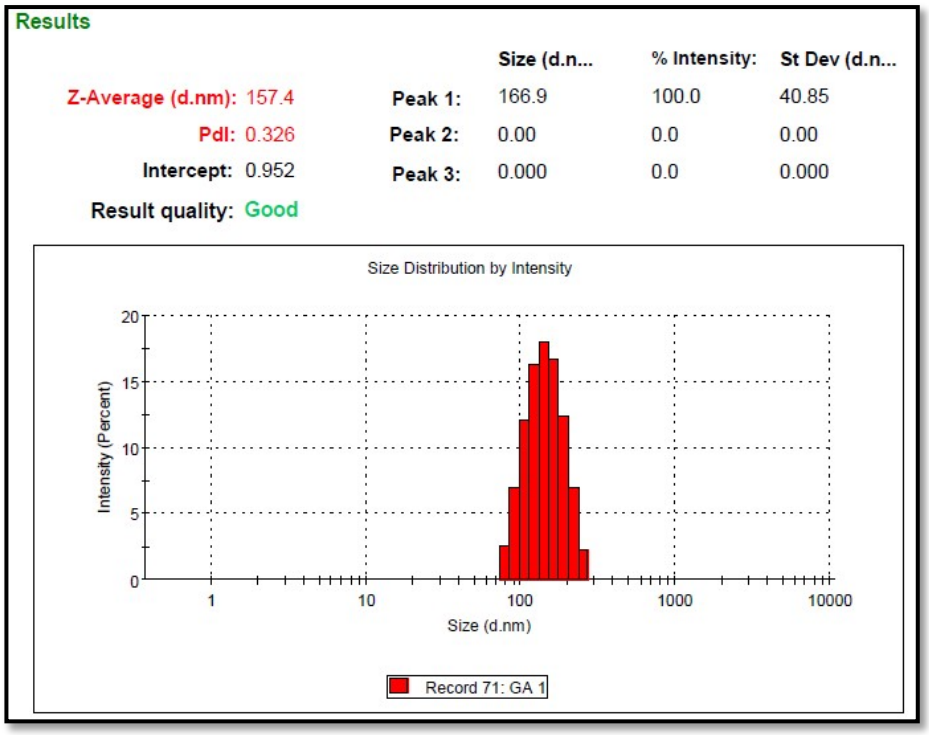

Figure- 5.14. Vesicle size of ATO loaded glycerosomes

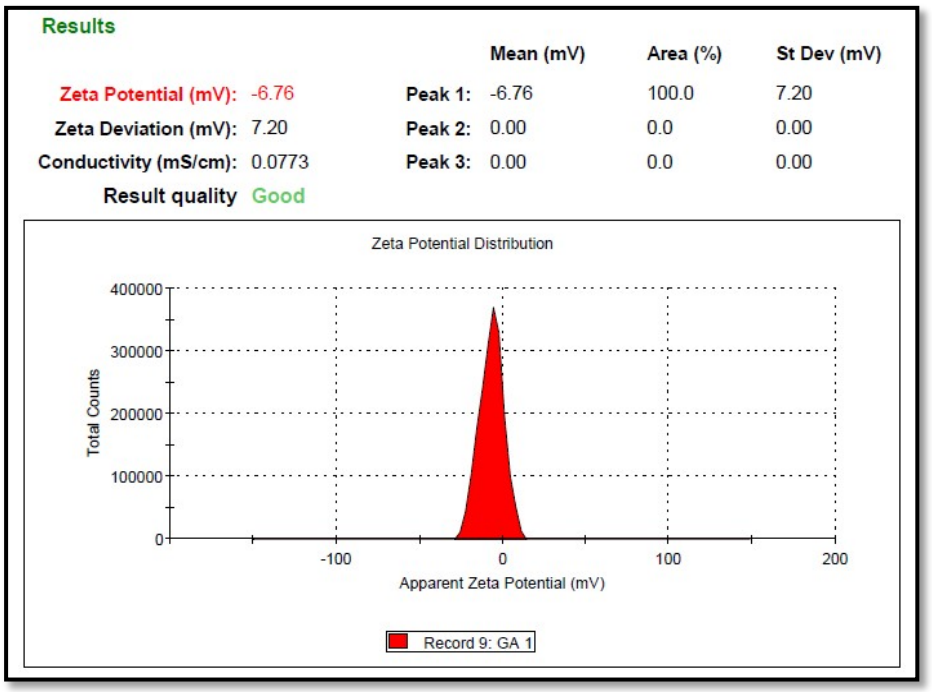

Figure- 5.15. Zeta potential of ATO loaded glycerosomes

5.19.2. Entrapment efficiency and % DLC:

The % entrapment efficiency was found to be 88.81 ± 2.33 % and drug loading capacity was found to be 11.00 ± 0.073 %.

5.19.3. Surface morphological study:

The surface morphology of ATO loaded glycerosomes as analysed by TEM is shown in figure- 5.16. The TEM photograph revealed smooth vesicles that are spherical in shape, small and uniform in size, vesicular in nature without agglomeration and homogeneously dispersed in medium with no disruptions of structure confirm vesicle integrity. The TEM image revealed vesicle size in range of 50 to 200 nm which was matched with vesicle size obtained from DLS.

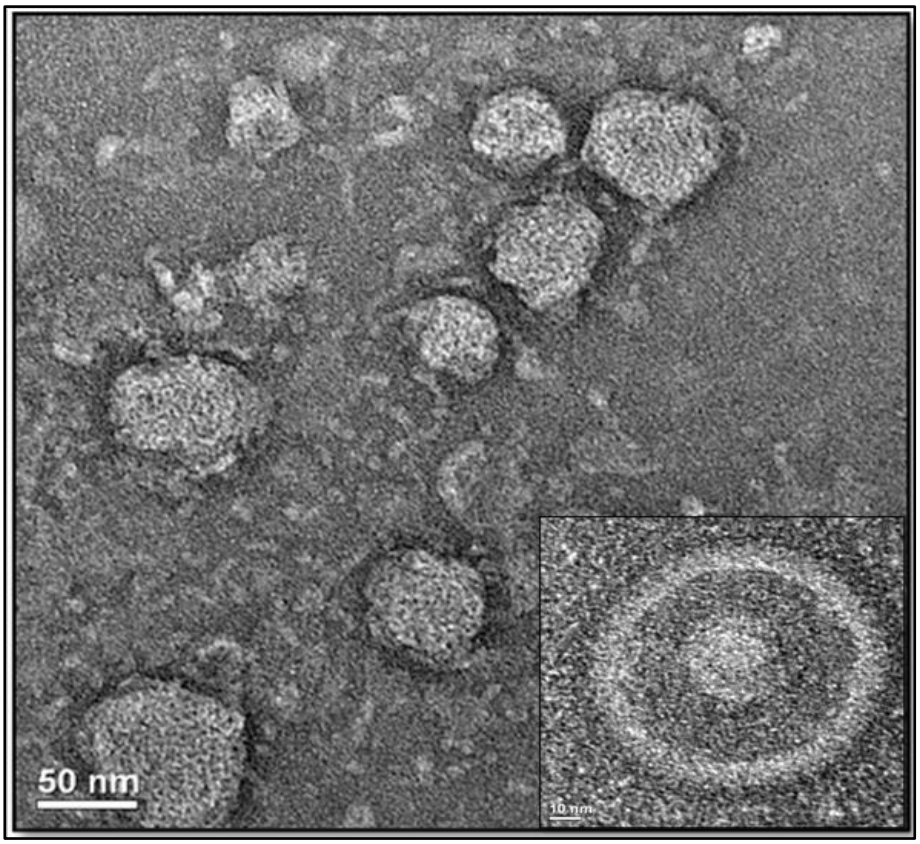

Figure- 5.16. TEM photograph of ATO loaded glycerosomes
(Inset image shows single vesicle)

5.19.4. FTIR Study:

The FTIR spectra of ATO and ATO loaded glycerosomes are shown in figure- 5.17. The spectra of ATO represents broad band in domain of 3650-2850 cm^{-1}, due to presence of water, which is superimposed over other characteristics peaks, like at 3381.21 cm^{-1} for -OH stretching, at 3363.85 cm^{-1} for -NH stretching and at 3055.24 cm^{-1} for -CH stretching. The other characteristic peaks found at 1656.85 cm^{-1} represent C=O stretching for amide carbonyl and 1683.86 cm^{-1} for carboxylate, 1317.38 cm^{-1} represent C-N stretching, 1523.76

cm^{-1} for N-H in plane bending (angular deformation) and 1215.15 cm^{-1} represent C-F stretching. All characteristic peaks of atorvastatin were retained with minor change in peak intensity in FTIR spectra of ATO loaded glycerosomes suggesting that ATO maintained its structural integrity.

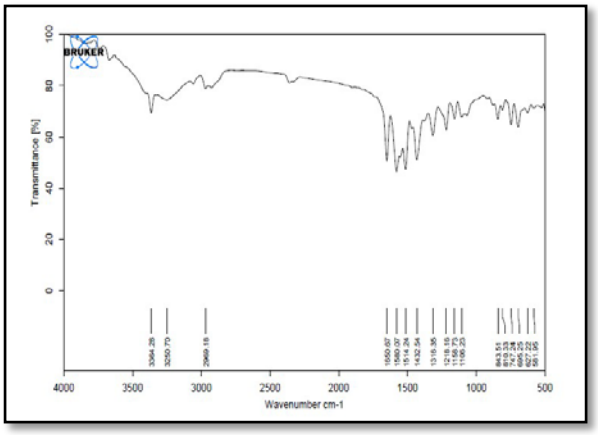

Figure 5.17a- FTIR spectra of Atorvastatin.

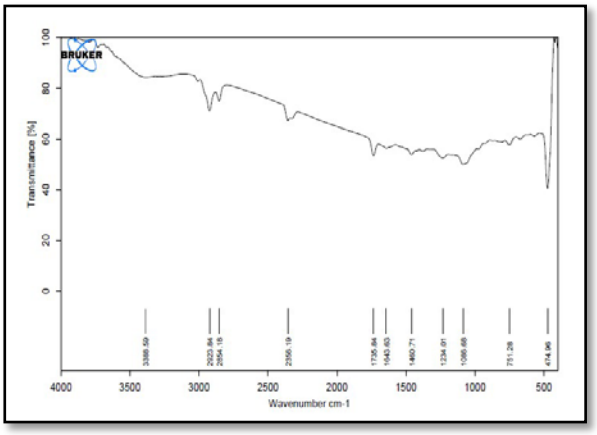

Figure 5.17b- FTIR spectra of Atorvastatin loaded glycerosomes

5.19.5. Residual solvent study:

The chromatogram of standard chloroform and methanol showed peak areas of 1437.47 and 1224.41 µg/mL respectively. According to ICH guidelines Q3C for residual solvent, Chloroform, and methanol limits upto 600 µg/mL/day and 3000 µg/mL/day respectively is considered as safe. The residue of methanol was found to be 5.17 µg/mL, while the residue of chloroform in ATO loaded glycerosomes was found to be 5.48 µg/mL. It was concluded that chloroform and methanol are present much below their safety limit in the prepared formulations and considered safe for further use.

5.20. Optimization and impact of glycerol concentration on physicochemical characterization of ATO loaded glycerosomes:

During this experimental work, preparation of glycerosomes was done by lipidic thin film hydration method and the study effect of glycerol concentration on its physicochemical characteristics viz. average vesicles size, size distribution, surface charge, entrapment efficiency, deformability index is shown in table- 5.23.

Table- 5.23. Characterization of ATO loaded glycerosomes

Glycerol concentration (% w/w)	Vesicle Size (d.nm)	PDI	Zeta Potential (mV)	% EE	% DLC	DI (%)
0 ($AGLY_0$)	113.0 ± 3.35	0.303± 0.089	-3.81± 0.69	80.03± 1.19	10.03 ± 0.128	12.70 ± 1.107
10 ($AGLY_{10}$)	137.3± 3.98	0.360± 0.122	-4.44± 0.63	83.98± 2.03	10.44 ± 0.095	16.21 ± 1.249
20 ($AGLY_{20}$)	159.75± 5.82	0.350± 0.106	-6.08± 0.66	88.81± 2.33	11.00 ± 0.073	21.23 ± 1.659
30 ($AGLY_{30}$)	161.6± 5.19	0.292± 0.048	-6.76± 0.98	90.77± 1.27	11.18 ± 0.103	31.74 ± 2.769

(n=3, ± S.D.)

*PDI- Polydispersity Index, % EE- % Entrapment efficiency, % DLC- Drug loading capacity, DI- Deformability Index.

As shown in table- 5.23, glycerosomes showed vesicle size ranging in between 113.0 to 161.6 d. nm and size distribution ranging between 0.292 to 0.403 (PDI). The results showed that the increase in concentration of glycerol increases vesicle size might be due to sticky nature of glycerol in glycerosomes [3, 9]. Glycerol increased the viscosity of the dispersion, rendering size reduction during sonication difficult, resulting in increase in vesicle size.

From the table-5.23, it was revealed that all formulations were able to entrap large amount of drug in vesicles ranging between 80.03 to 90.77 %. From the results it was observed that increase in concentration of glycerol increases EE of drug due to glycerol probably allowed better packing of lipid bilayer which resisted drug leakage from the vesicles leading to increased EE [56]. High drug loading capacity was observed in glycerosomes ranging in between 10.03 to 11.18 %.

Zeta potential of all formulation was found to be in between -3.81 to -6.76 mV. The zeta potential increases with increased in concentration of glycerol. This might be explained by a specific interaction between glycerol and the polar heads of phospholipids, which would modify the orientation of molecules and ultimately have an impact on the system's overall surface charge [57]. The DI increased with increased in the concentration of glycerol resulting in more elasticity and deformability to lipidic bilayer of glycerosomes. The increase in DI could be attributed to the ability

of glycerol to act as an edge activator for phospholipid bilayers, especially at high concentrations (more than 20%w/w) [58].

5.21. Rheological studies:

Figure- 5.18a represents the graph of shear rate vs shear stress (τ). Figure- 5.18b represents the change in viscosity (η) as a function of shear rate, and figure- 5.18c represents the in the logarithmic form of shear rate as a function of logarithmic form of viscosity (η).

The results (figure-5.18a) clearly reveal that shear stress increases linearly as shear rate increases, indicating Newtonian behaviour of glycerosomal formulations. From the results (Figure 5.18b), pseudoplastic or shear thinning behaviour was observed. The decreasing order of viscosity of glycerosomes is as follows: $Gly_{30} > Gly_{20} > Gly_{10} > Gly_0$. By extrapolating the viscosity data, we can determine the zero-shear viscosity (η_0) of the combined systems.

The viscosity (η_0) of Gly_0, Gly_{10}, Gly_{20} and Gly_{30} at zero-shear viscosity (η_0) was found to be 120.54, 136.75, 232.68 and 301.99 mpas respectively. The apparent viscosity (K) was used as the proportionality constant. Table- 5.24 summarized the values of n, K, and R^2 (statistical correlation coefficient) produced from fitting of shear rate vs shear stress data. Based on results of K and η_0, it was observed that the viscosity was increased with increase in glycerol concentration. The flow behaviour index (n) is a measure of a system's deviation from Newtonian behaviour. If n < 1, it denotes pseudoplastic flow or shear thinning; n = 1 denotes Newtonian behaviour; and n > 1 denotes dilatant or shear thickening. The value of "n" in glycerosomes is smaller than 1, hence, glycerosomes formulation exhibits shear thinning and is suitable for transdermal administration [59-61].

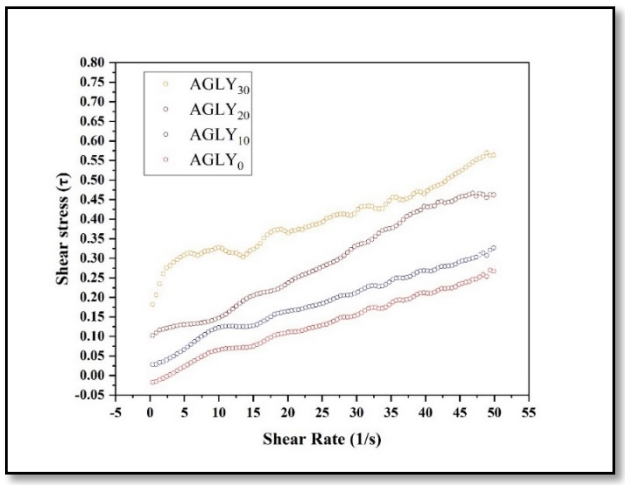

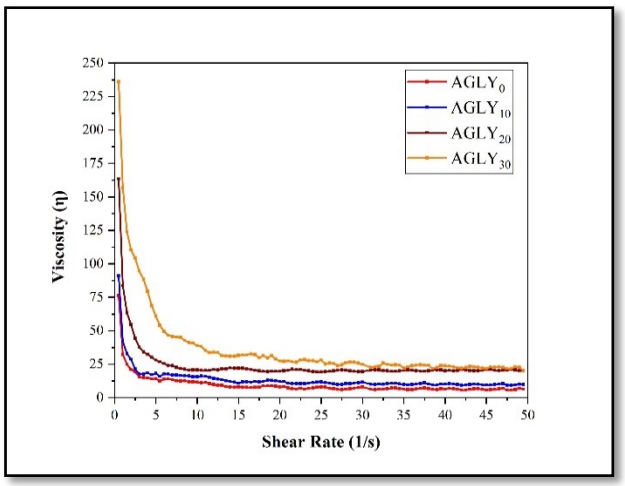

a. Shear rate Vs shear stress (τ) b. Shear rate Vs Viscosity (η)

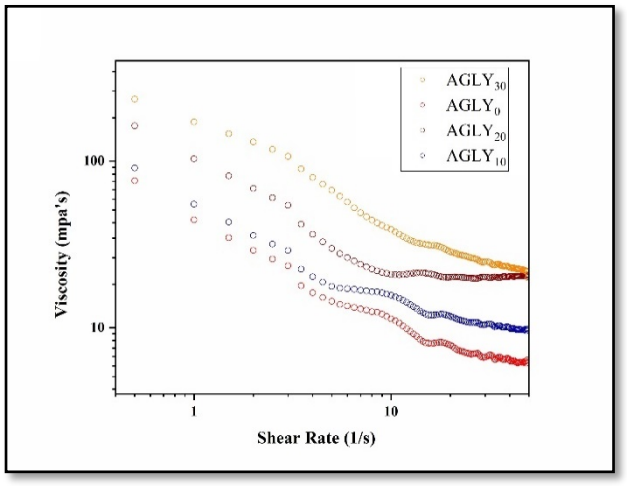

c. Logarithmic form of shear rate and viscosity (η).

Figure- 5.18. Different graph for rheological studies.

a. Shear rate Vs shear stress (τ)
b. Shear rate Vs Viscosity (η)
c. Logarithmic form of shear rate and viscosity (η)

Table- 5.24. Rheological power law fitting parameters for glycerosomes

Formulations	η_0	K	n	R^2
$AGLY_0$	120.54	76.40	0.68	0.9925
$AGLY_{10}$	136.75	87.77	0.64	0.9875
$AGLY_{20}$	232.68	162.85	0.84	0.9896
$AGLY_{30}$	301.99	242.69	0.35	0.9824

5.22. *In vitro* drug release study:

The release of drug from pure drug and ATO loaded glycerosomes containing different concentration of glycerol from 0% (conventional liposomes) to 30 % w/w to check effect of glycerol concentration on drug release in PBS pH 5.5 and PBS pH 7.4 is represented in figure- 5.19. From the results (table- 5.26), it was observed that 98.85 % of ATO released from the pure drug within 8 hrs, while 98.39 % of drug released from ATO loaded liposomes i.e., $AGLY_0$ within 48 hrs. The results from figure- 5.19 (b) showed 95.17 %, 90.70 %, 83.96 % of cumulative drug release from $AGLY_{10}$, $AGLY_{20}$ and $AGLY_{30}$ within 48 hrs. The results revealed that as concentration of glycerol increases, there is decrease in drug release which

might be attributed to osmotic and hygroscopic property of glycerol [42, 43]. The sustained drug release with an increase in glycerol concentration is due to a decrease in available surface area (diffusion area) for drug release due to an increase in vesicle size, as previously mentioned [1, 4]. Indeed, the size of the vesicle had a significant impact on drug release from glycerosomes. The rate of drug release from small-size vesicles was higher as compared to large-size vesicles, because the drug molecules are more easily accessible to the medium and can diffused out of the vesicles more quickly [43]. From the above results, it was concluded that the glycerosomes showed sustained drug release than liposomes (0% w/w glycerosomes) and pure drug.

The drug release in saline phosphate buffer pH 5.5 is represented in figure-5.19 (a) and table-6.25. From the results, it was observed that 99.66 % of ATO released from the pure drug within 8 hrs, while 85.16 %, 78.43 %, 72.88 % and 70.06% of cumulative drug released from $AGLY_0$, $AGLY_{10}$, $AGLY_{20}$ and $AGLY_{30}$ within 48 hrs in PBS pH 5.5 which represents the pH of skin layers. The release of drug from the formulation in PBS pH 5.5 was more sustained as compared to the release observed in PBS pH 7.4. This might be due to the low solubility of ATO at pH 5.5 as compared to pH 7.4. Hence, the drug required more time to release from the formulation and diffused from the dialysis membrane into the receptor compartment. The more sustained release of drug at pH 5.5, i.e., skin pH, may serve as a local depot for sustained release.

The data obtained from in-vitro drug release studies was fitted to the various release models like Zero-order, First order, Higuchi model and Korsmeyer-Peppas model. The regression-coefficient of the plot of zero order kinetic for pure drug was found to be 0.9881, while regression-coefficient of the plot of first order release model for ATO loaded liposomes ($AGLY_0$) was found to be 0.9790. The regression-coefficient of the plot of first order release model for $AGLY_{10}$, $AGLY_{20}$ and $AGLY_{30}$ were found to be 0.9918, 0.9959 and 0.9909 respectively. The release pattern follows anomalous transport release mechanism ($n > 0.5$) for all glycerosomes formulation (10-30% w/w glycerol concentration) and liposomes (0% w/w glycerol concentration) in PBS 7.4. The release exponent was found to be greater than 0.5 in PBS pH 7.4 as well as PBS pH 5.5 (shown in table- 5.27 and 5.28) for ATO loaded glycerosomes indicated that drug release follows diffusion-controlled release mechanism.

In case of PBS 5.5, the regression-coefficient of the plot of zero order release model for pure drug was found to be 0.9810, while regression-coefficient of the plot of Higuchi model for ATO loaded liposomes ($AGLY_0$) was found to be 0.9578. The regression-coefficient of the

plot of Higuchi model for $AGLY_{10}$, $AGLY_{20}$ and $AGLY_{30}$ were found to be 0.9675, 0.9648 and 0.9707 respectively. In PBS 5.5, the release pattern followed non fickian diffusion release mechanism for ATO loaded glycerosomes (n>0.5).

Table- 5.25. *In vitro* drug release profile for ATO loaded glycerosomes in PBS pH 5.5

Time (In Hrs)	**Pure ATO**	**$AGLY_0$**	**$AGLY_{10}$**	**$AGLY_{20}$**	**$AGLY_{30}$**
0	0 ± 0	0 ± 0	0 ± 0	0 ± 0	0 ± 0
0.5	19.31 ± 0.65	2.05 ± 0.90	0.85 ± 0.42	0.51 ± 0.18	0.2 ± 0.1
1	30.20 ± 1.05	4.21 ± 1.23	3.97 ± 0.98	2.53 ± 0.52	2.31 ± 0.99
1.5	38.21 ± 2.00	7.81 ± 2.57	7.09 ± 1.32	4.38 ± 0.92	4.01 ± 0.79
2	46.58 ± 0.89	11.18 ± 2.63	8.29 ± 2.26	7.71 ± 0.88	5.61 ± 1.02
3	58.02 ± 1.20	14.54 ± 0.36	12.62 ± 2.37	10.54 ± 1.11	9.25 ± 1.23
4	70.32 ± 0.96	17.18 ± 1.50	16.23 ± 2.28	13.63 ± 0.88	11.89 ± 2.12
5	78.52 ± 1.96	20.79 ± 1.33	19.35 ± 1.22	18.01 ± 1.46	16.85 ± 1.53
6	91.98 ± 1.12	26.07 ± 2.81	25.35 ± 1.15	22.46 ± 1.11	21.57 ± 1.36
8	99.66 ± 0.71	36.41 ± 2.43	32.44 ± 1.15	29.67 ± 2.38	26.01 ± 1.32
10		44.35 ± 1.81	38.22 ± 1.48	35.58 ± 1.63	30.34 ± 2.28
12		50.61 ± 1.88	44.11 ± 2.53	40.51 ± 1.89	36.82 ± 2.61
24		74.35 ± 2.01	65.61 ± 2.46	60.86 ± 2.39	56.46 ± 3.19
48		85.16 ± 2.86	78.43 ± 3.00	72.88 ± 2.48	70.06 ± 2.04

(n=3, ±S.D.)

Table- 5.26. *In vitro* drug release profile of ATO loaded glycerosomes in PBS pH 7.4

Time (In Hrs)	Pure ATO	AGLY$_0$	AGLY$_{10}$	AGLY$_{20}$	AGLY$_{30}$
0	0 ± 0	0 ± 0	0 ± 0	0 ± 0	0 ± 0
0.5	21.96 ± 2.59	11.89 ± 1.03	8.04 ± 0.77	7.21 ± 0.83	5.17 ± 0.41
1	30.24 ± 2.03	18.22 ± 0.56	12.01 ± 0.58	9.25 ± 0.74	8.97 ± 0.77
1.5	36.76 ± 1.34	22.78 ± 0.68	15.72 ± 1.00	13.38 ± 0.53	11.54 ± 0.85
2	42.72 ± 1.09	27.67 ± 2.26	17.24 ± 0.85	15.30 ± 1.01	13.82 ± 0.64
3	51.82 ± 1.21	34.21 ± 1.41	22.52 ± 0.86	19.03 ± 0.58	17.67 ± 0.95
4	61.48 ± 0.68	42.81 ± 1.66	26.9 ± 1.62	21.96 ± 0.77	19.20 ± 0.72
5	70.65 ± 0.93	47.94 ± 1.59	30.96 ± 0.82	26.59 ± 0.94	22.41 ± 0.51
6	82.74 ± 1.17	51.15 ± 0.94	36.97 ± 1.90	30.72 ± 0.91	25.02 ± 0.84
8	98.85 ± 0.89	56.32 ± 0.65	44.88 ± 1.07	38.17 ± 1.20	32.12 ± 1.97
10		67.21 ± 0.85	53.93 ± 1.27	48.70 ± 1.37	41.17 ± 1.10
12		71.21 ± 1.69	59.69 ± 1.12	56.23 ± 2.51	48.39 ± 2.34
24		85.42 ± 1.99	76.58 ± 1.77	71.43 ± 2.15	64.20 ± 1.88
48		98.39 ± 1.00	95.17 ± 1.10	90.71 ± 1.86	83.96 ± 1.03

(n=3, ±S.D.)

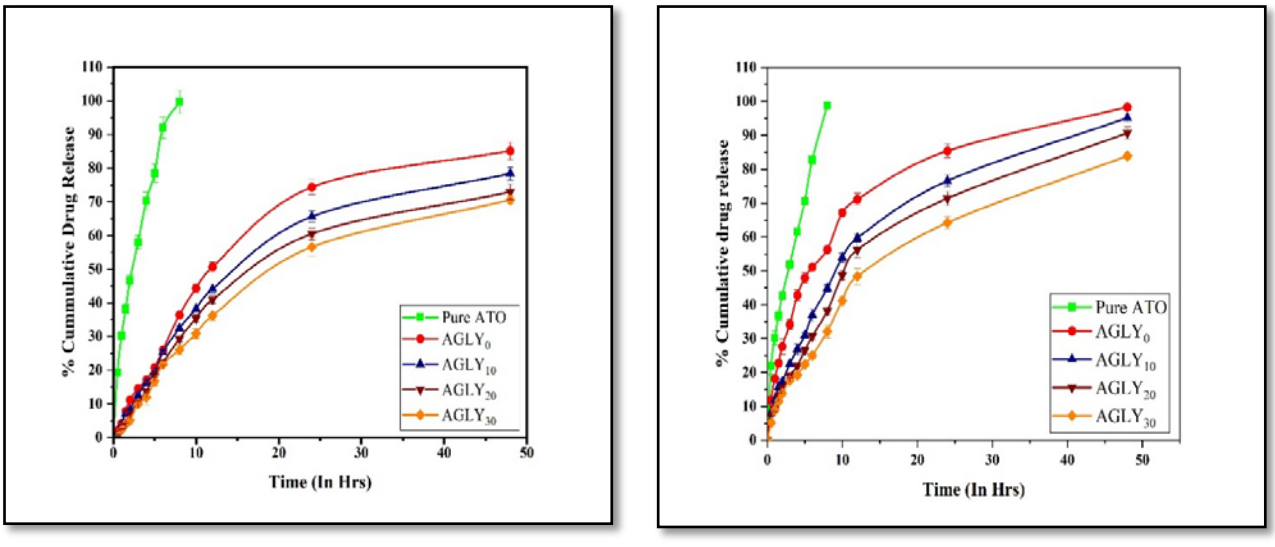

(a) (b)

Figure- 5.19. Comparison of % cumulative drug release of Pure ATO and ATO loaded glycerosomes containing different glycerol concentration (0-30% w/w) in (a) pH 5.5 and (b) pH 7.4.

Table- 5.27. Drug release kinetic models for ATO loaded glycerosomes in PBS pH 5.5

Kinetic Models	Pure ATO	$AGLY_0$	$AGLY_{10}$	$AGLY_{20}$	$AGLY_{30}$
Zero order	**0.9810**	0.8377	0.8512	0.8524	0.8792
First order	0.7600	0.9568	0.9606	0.9504	0.9639
Higuchi	0.9796	**0.9578**	**0.9675**	**0.9648**	**0.9707**
Korsemeyer-Peppas (n)	0.4989 **(0.606)**	0.8786 **(0.662)**	0.8914 **(0.654)**	0.9223 **(0.727)**	0.9226 **(0.801)**

Table- 5.28. Drug release kinetic models for ATO loaded glycerosomes in PBS pH 7.4

Kinetic Models	Pure ATO	$AGLY_0$	$AGLY_{10}$	$AGLY_{20}$	$AGLY_{30}$
Zero order	**0.9790**	0.7021	0.8208	0.8450	0.8781
First order	0.8511	**0.9918**	**0.9959**	**0.9909**	**0.9881**
Higuchi	0.9758	0.9305	0.9742	0.9745	0.9822
Korsemeyer-Peppas (n)	0.5671 **(0.381)**	0.5732 **(0.691)**	0.9853 **(0.489)**	0.7304 **(0.526)**	0.7631 **(0.554)**

5.23. *Ex vivo* skin permeation study:

The results of *ex vivo* skin permeation study are shown in table-5.29 and figure-5.20. Conventional liposomes ($AGLY_0$) and pure drug were used as controls. The % cumulative amount of drug permeated through rat skin were calculated and plotted against time during 48 hrs experiment. The % amount of drug permeated through skin from pure drug after 48 hrs was 36.92 %, while 58.55 % drug was permeated by ATO loaded liposomes. The % amount of drug permeated through skin from $AGLY_{10}$, $AGLY_{20}$ and $AGLY_{30}$ after 48 hrs was 69.05, 72.30 and 82.46% respectively. Thus, the amount of drug delivered through skin by ATO loaded glycerosomes using $AGLY_{30}$, $AGLY_{20}$ and $AGLY_{10}$ were enhanced 2.97-, 2.34- and 1.75- folds in comparison with pure drug respectively while 1.53-, 1.18- and 0.88- folds as compared to ATO loaded liposomes ($AGLY_0$). From the results of permeation profile, it was revealed that the amount of ATO was permeated through the skin was higher for glycerosomes as compared to liposomes and pure drug. AGLY30 gave a higher drug permeation rate due to the higher deformability and elastic nature of the vesicles and fluidity of the phospholipid bilayer of the glycerosomes also allowed them to travel easily through the biological membrane [2, 13, 43, 62, 63]. The presence of glycerol confers flexibility to the bilayer and hydrate the skin due to

humectant property of glycerol. These properties of glycerol help mitigate the skin's natural barrier, which enhances the permeability of vesicles through the skin.

The results of the skin deposition study showed that in the case of pure drug, the maximum amount of drug remained on the skin, indicating that drug alone is unable to cross the skin barrier efficiently due to low solubility and poor permeability. In the case of $AGLY_0$, the drug deposition was higher as compared to pure drug due to the less elastic nature of the vesicles and the greater attraction of the phospholipids of the vesicles towards the skin lipids present abundantly in the outer layer of skin. The skin deposition of glycerosomes decreased with an increase in glycerol concentration (i.e., $AGLY_{30} < AGLY_{20} < AGLY_{10}$). The more $AGLY_{20}$ and $AGLY_{10}$ were accumulated, the more drug was accumulated drug into the skin, where it acts as a depot for sustained drug release. The $AGLY_{30}$ showed minimal remained on the skin and deposited in the skin due to the elastic nature and higher deformability of vesicles, which facilitated permeation easily through the skin and avoided retention in the skin.

The flux was calculated from the slope of the linear portion of the plot and denoted as J. The average flux (amount of drug permeated per area per time; $\mu g/cm^2/hr$) of pure drug was found to be 11.01 $\mu g/cm^2/hr$ while the average flux for $AGLY_{30}$, $AGLY_{20}$, $AGLY_{10}$ and $AGLY_0$ was found to be 32.48, 25.79, 19.17 and 21.81 $\mu g/cm^2/hr$ respectively and it was higher as compared to pure drug. The transdermal flux was found in an increasing order of $AGLY_{30} > AGLY_{20} > AGLY_0 > AGLY_{10}$ > pure drug. From the results, it was found that the transdermal flux increased with an increase in glycerol concentration due to an enhanced deformable index of vesicles with an increase in glycerol concentration. The steady state flux of pure drug and ATO loaded liposomes ($AGLY_0$) was found to be 10.17 and 13.84 $\mu g/cm^2/hr$, while steady state flux for $AGLY_{10}$, $AGLY_{20}$ and $AGLY_{30}$ was found to be 17.06, 17.93 and 21.19 $\mu g/cm^2/hr$. On the basis of the results, it was concluded that an increase in the concentration of glycerol increases the permeation of the drug through skin layers.

Table- 5.29. *Ex vivo* skin permeation profile of ATO loaded glycerosomes

Time (In hrs)	$AGLY_{30}$	$AGLY_{20}$	$AGLY_{10}$	$AGLY_{0}$	Pure ATO
0	0 ± 0	0 ± 0	0 ± 0	0 ± 0	0 ± 0
0.5	0.40 ± 0.31	0.14 ± 0.06	0 ± 0	0.08 ± 0.02	0 ± 0
1	2.87 ± 0.83	1.82 ± 0.43	0.71 ± 0.19	1.03 ± 0.15	0 ± 0
2	6.07 ± 0.66	4.08 ± 0.71	2.6 ± 0.44	4.13 ± 0.71	1.24 ± 0.25
3	9.45 ± 1.01	6.50 ± 0.41	4.66 ± 0.35	6.97 ± 0.48	1.87 ± 0.32
4	11.3 ± 0.80	10.29 ± 1.09	7.08 ± 0.67	9.03 ± 0.35	3.39 ± 0.66
5	15.58 ± 1.32	13.21 ± 0.48	9.51 ± 0.72	12.31 ± 1.07	5.55 ± 0.63
6	19.39 ± 1.05	16.70 ± 0.73	12.0 ± 1.47	15.01 ± 0.88	7.77 ± 0.94
7	23.95 ± 1.67	21.88 ± 1.14	13.76 ± 1.03	17.61 ± 1.26	10.67 ± 0.67
8	29.05 ± 2.28	23.72 ± 0.78	17.2 ± 0.84	19.92 ± 1.39	11.55 ± 0.98
10	38.49 ± 1.89	28.84 ± 0.56	24.96 ± 0.91	22.95 ± 0.66	14.29 ± 1.19
12	47.46 ± 2.43	34.18 ± 1.30	28.72 ± 1.61	27.05 ± 1.67	18.9 ± 1.05
24	61.79 ± 2.15	48.46 ± 0.65	42.25 ± 2.11	40.52 ± 1.51	27.83 ± 0.71
30	72.05 ± 1.11	58.39 ± 1.89	56.54 ± 2.06	44.37 ± 1.86	31.59 ± 0.71
48	82.46 ± 2.38	72.30 ± 2.26	65.05 ± 2.62	56.55 ± 2.01	36.92 ± 0.94

Parameters	$AGLY_{30}$	$AGLY_{20}$	$AGLY_{10}$	$AGLY_{0}$	Pure ATO
Drug remained on skin (%)	5.56 ± 0.68	19.86 ± 2.15	25.89 ± 2.02	27.53 ± 1.61	56.92 ± 2.75
Drug retained in skin (%)	8.43 ± 1.04	7.95 ± 0.98	8.19 ± 1.22	13.80 ± 1.78	4.19 ± 0.99
Transdermal flux (µg/cm²/hr)	32.48	25.79	19.17	21.81	11.01
Steady state flux (J_{ss})	21.19	17.93	17.06	13.84	10.17
PER (as compared to pure drug)	2.97	2.34	1.75	1.97	1.00
PER (as compared to liposomes)	1.53	1.18	0.88	1.00	-

(n=3, ±S.D.)

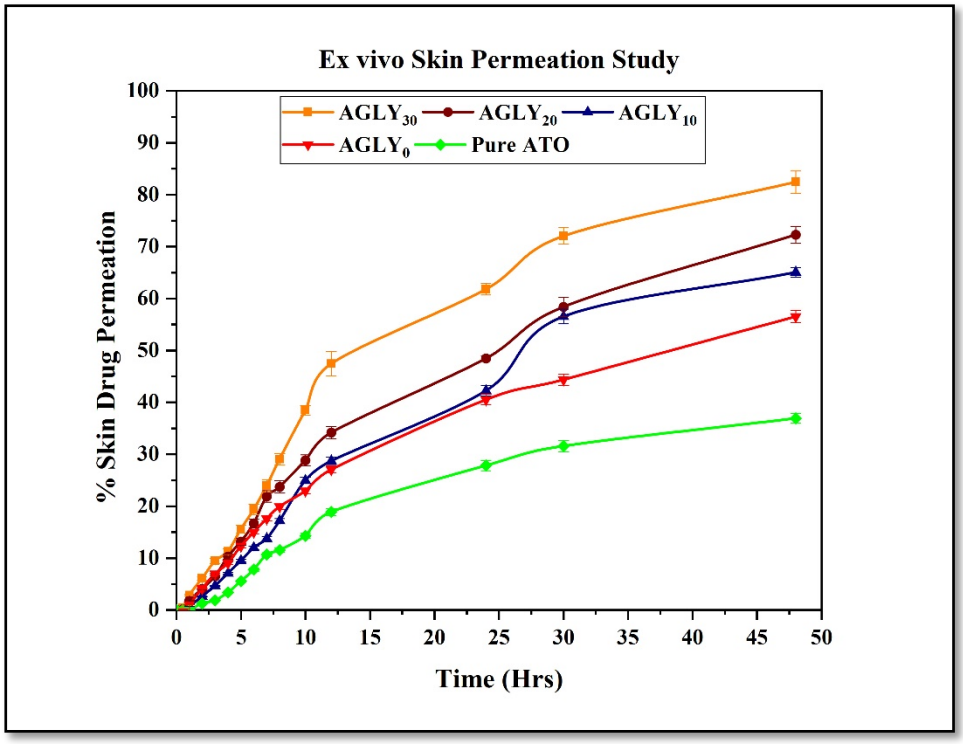

Figure- 5.20. Comparison of % cumulative drug permeation of pure ATO and ATO loaded glycerosomes containing different glycerol concentration.

5.24. Optimization of glycerol concentration in ATO loaded glycerosomes:

On the basis of results of physicochemical characteristics, *in vitro* drug release and *ex vivo* skin permeation studies of ATO loaded glycerosomes, it was revealed that the 30% w/w glycerol containing ATO loaded glycerosomes showed better skin permeation (shown in figure- 5.20 and table- 5.29), sustained drug release (shown in table- 5.25 & 5.26 and figure- 5.19), higher entrapment efficiency, drug loading capacity, and higher deformability index of glycerosomes (shown in table- 5.23). On the basis of above experimental results, 30 % w/w glycerol containing ATO loaded glycerosomes ($AGLY_{30}$) was optimized and chosen for further *in vitro* cell line studies, *ex vivo* studies, stability studies and in vivo pharmacokinetic and pharmacodynamic studies.

5.25. *In vitro* cell viability study:

When studying new drug delivery system, the *in vitro* cell viability study is an important aspect to evaluate its safety. The cell viability study was assessed by performing the MTT test. Placebo glycerosomes, placebo liposomes, pure drug, ATO loaded liposomes ($AGLY_0$) and ATO loaded glycerosomes ($AGLY_{30}$) were exposed to fibroblast cells at different incubation time (12 and 24 hrs) using PBS 7.4 as positive control and Triton X100 as a negative control. The

results of cell viability study (figure- 5.21) showed that no reduction in cell viability for placebo glycerosomes was observed; while, ATO loaded glycerosomes showed slight reduction in cell viability after 12 and 24 hrs treatment due to release of drug from the formulation The placebo liposomes and placebo glycerosomes showed no remarkable changes in the cell viability. In case of pure drug, reduction in the viability was observed at 24 hrs exposure time. In the cells incubated with pure drug, cell mortality was found to be more than 10% in 24 hrs. It was observed that the cell viability decreased with increased in the concentration of pure drug from 50 to 250 µM. The cell mortality after treatment of ATO loaded glycerosomes and liposomes were found to be very low (less than 10%) upto 24 hrs treatments. Also, the cell viability of glycerosomes was higher as compared to liposomes due to the more sustained release of drug from the glycerosomes as compared to liposomes. From the results, it was concluded that glycerosomes are considered safe nanocarriers for transdermal drug delivery.

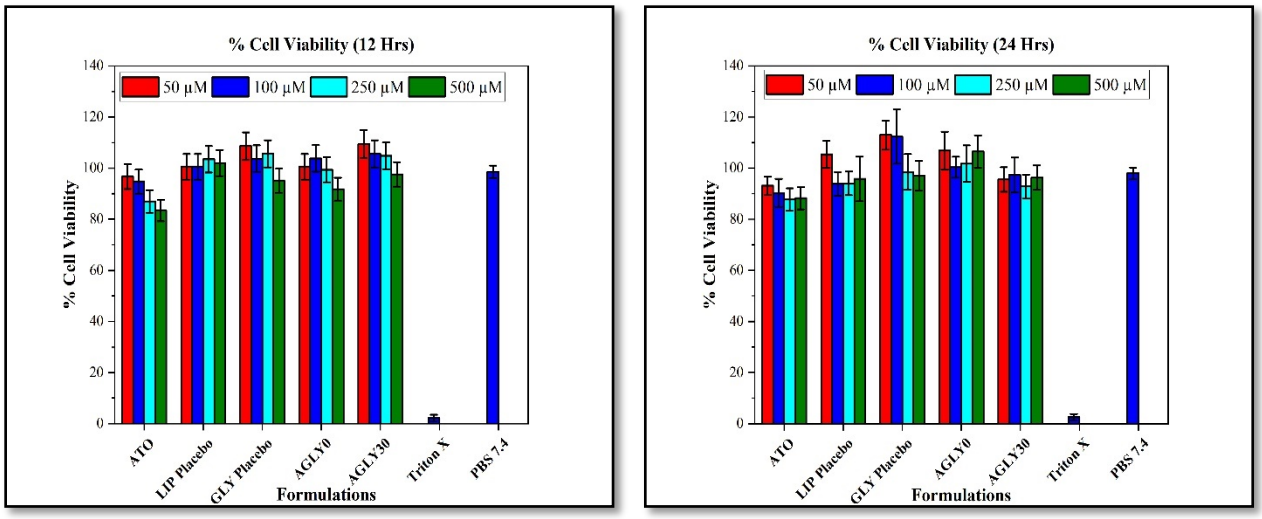

(a) (b)

Figure- 5.21. % cell viability study (a) 12 hrs and (b) 24 hrs.

5.26. *In vitro* cell permeability study:

The stratum corneum layer of skin is a rate limiting barrier for permeation of drug through skin layers. The integrity of cell monolayer cultured for 21-25 days was regularly monitored by measuring the TEER value. The TEER values of monolayer in range of 500-1100 Ωcm^2 were accepted to use for transport mechanism. Transcellular permeation of formulations through human keratinocytes monolayer was determined. If apparent permeability coefficient (P_{app}) of substances is less than 1 X 10^{-6}cm/s considered as low permeable substances, while high permeable substances exhibit apparent permeability coefficients value of higher than 1 X 10^{-5} cm/s [34-36].

The TEER value for cell permeability was found to be 970-1000 Ωcm^2 and it showed good quality of development of monolayer on basement. The results of cell permeability study for pure drug, ATO loaded liposomes and ATO loaded glycerosomes are shown in table- 5.30 and figure-5.22. For pure drug, P_{app} value was found to be 7.83 $\times 10^{-6}$ cm/s and it was considered low-medium permeable. While, ATO loaded liposomes and ATO loaded glycerosomes exhibited P_{app} value of 1.17 $\times$ 10^{-5} cm/s and 1.80$\times 10^{-5}$ cm/s respectively. On the basis of result, it was concluded that the glycerosomes showed medium to high permeability as compared to pure drug and ATO loaded liposomes. This might be due to the nanosize of formulations and the presence of glycerol, which increases the deformability and fluidity of vesicles and facilitates the permeation of drug-loaded vesicles through the cell layer [2, 55]. The hydrophobic tails of the phospholipids in the membrane might interact with glycerol, causing them to disorganize resulting in additional space between them. Drugs can pass through the membrane more easily as a consequence of the membrane being more fluid and flexible. Overall, glycerol can improve drug delivery and effectiveness by increasing membrane fluidity and solubilizing hydrophobic drugs, which can boost drug transport across artificial cell membranes. From the results, it was concluded that the permeability of ATO through cell layer was enhanced by ATO loaded glycerosomes.

Table- 5.30. *In vitro* cell permeability profile

Time (In Hrs)	**Pure ATO**	**AGLY$_0$**	**AGLY$_{30}$**
0	0 ± 0	0 ± 0	0 ± 0
1	17.61 ± 2.47	21.81 ± 1.71	32.81 ± 3.02
2	24.65 ± 1.64	33.01 ± 4.48	51.40 ± 5.39
3	35.04 ± 3.04	52.52 ± 3.18	81.23 ± 4.47
4	40.78 ± 3.33	68.20 ± 4.32	97.18 ± 1.77
6	52.56 ± 5.85	84.59 ± 2.88	
8	71.91 ± 2.88	99.40 ± 2.94	
12	88.81 ± 1.45		
P_{app} (cm/s)	7.83 $\times 10^{-6}$	1.17 $\times$ 10^{-5}	1.80$\times 10^{-5}$

(n=3, ±S.D.)

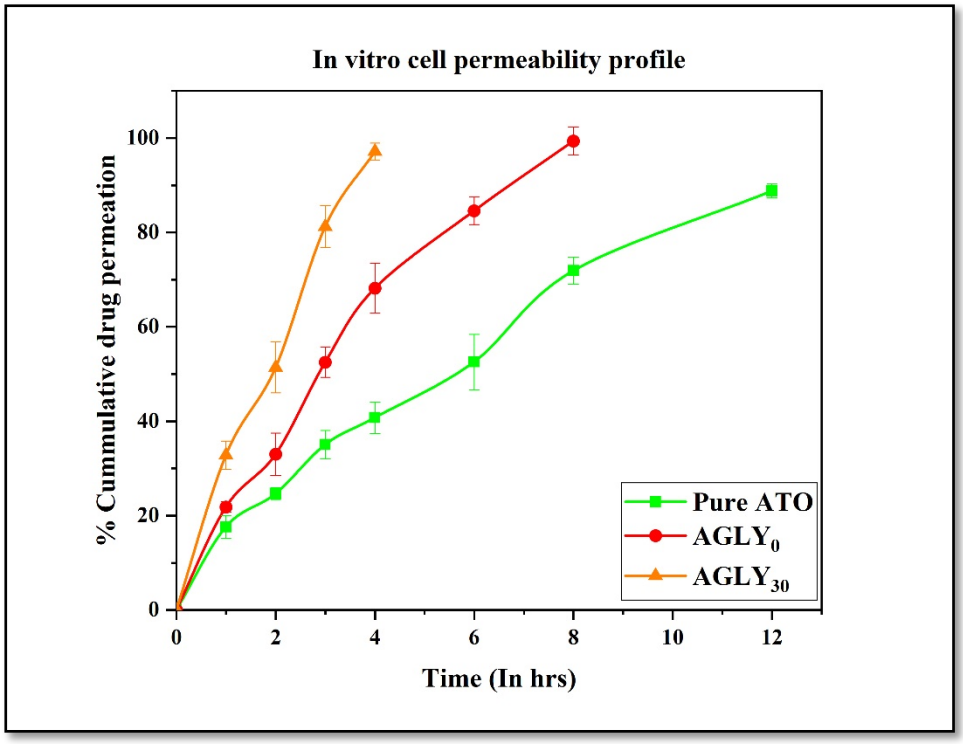

Figure- 5.22. *In vitro* cell permeability profile

5.27. Stability study:

The effect of storage conditions on physicochemical parameters like vesicle size and % assay is shown in table- 5.31 and figure- 5.23. Table-5.29 depicted that there was no significant change ($p > 0.05$) in vesicle size and % assay of glycerosomes ($AGLY_{30}$) formulation on storage at 2-8°C (Figure-5.23A and 5.23D) and 25±2°C/60±5 % RH (Figure-5.23B and 5.23E), indicating that the vesicles did not tend to aggregate or unite. There was slight increase in vesicle size and slight decrease in % assay at 40±2°C/75 ± 5% RH (Figure-5.23C and 5.23F). In case of 0% glycerosomes (liposomes), the average vesicle size was slightly increased and % assay was slightly decreased at both storage conditions (25±2°C/60 ± 5 % RH as well as 40±2°C/75 ± 5 % RH) but were stable at 2-8 °C. On the basis of results, it was concluded that ATO loaded glycerosomes were more stable than ATO loaded liposomes ($AGLY_0$) at both storage conditions (2-8 °C and 25±2°C/60 ± 5 % RH). The addition of glycerol enhanced the viscosity of the medium, reducing the chance of particle aggregation. Also the interaction of glycerol with the phospholipid resulted in an extra dense organisation of the vesicles, which hindered their mobility [64, 65]. On the basis of results, it was revealed that ATO loaded glycerosomes were more stable at 2-8 °C and 25±2°C/60 ± 5 % RH for more than 90 days as compared to ATO loaded liposomes.

Table- 5.31. Stability study profile

Sr. No.	Time interval (In Month)	Glycerosomes Batch	Vesicle Size (d.nm)			% Assay		
			2-8°C	25±2°C/60 ± 5 % RH	40±2°C/75 ± 5 % RH	2-8°C	25±2°C/60 ± 5 % RH	40±2°C/75 ± 5 % RH
1	Initial	$AGLY_0$	113.0 ± 3.35	113.0 ± 3.35	113.0 ± 3.35	99.13 ± 1.19	99.18 ± 1.19	99.18 ± 1.19
		$AGLY_{30}$	161.6 ± 5.19	161.6 ± 5.19	161.6 ± 5.19	99.77 ± 1.27	99.77 ± 1.27	99.77 ± 1.27
2	0.5	$AGLY_0$	115.1 ± 6.05	131.4 ± 4.92	138.4 ± 8.92	98.05 ± 0.9	98.15 ± 1.56	97.69 ± 0.47
		$AGLY_{30}$	158.8 ± 4.14	163.3 ± 2.23	164.6 ± 4.23	99.07 ± 1.05	97.71 ± 1.44	98.71 ± 0.85
3	1.0	$AGLY_0$	112.9 ± 4.75	128.9 ± 3.44	148.6 ± 9.45	96.24 ± 1.02	97.82 ± 1.85	94.87 ± 2.63
		$AGLY_{30}$	162.8 ± 2.04	160.3 ± 4.59	171.9 ± 7.59	98.65 ± 1.63	98.63 ± 0.57	93.63 ± 1.14
4	1.5	$AGLY_0$	122.4 ± 3.57	146.6 ± 5.12	182.6 ± 7.13	97.85 ± 1.26	94.79 ± 1.69	95.15 ± 1.82
		$AGLY_{30}$	165.8 ± 3.24	168.1 ± 5.95	179.1 ± 6.89	98.78 ± 2.02	97.69 ± 1.59	95.69 ± 2.02
5	2.0	$AGLY_0$	126.7 ± 8.69	163.9 ± 7.04	240.9 ± 10.15	96.45 ± 1.89	96.16 ± 2.15	90.09 ± 1.69
		$AGLY_{30}$	166.9 ± 4.35	172.6 ± 3.56	199.3 ± 8.56	98.88 ± 1.85	98.19 ± 1.74	92.19 ± 3.31
6	2.5	$AGLY_0$	123.6 ± 4.12	179.3 ± 6.25	220.3 ± 10.65	96.18 ± 2.58	95.23 ± 2.69	92.36 ± 2.62
		$AGLY_{30}$	164.3 ± 3.25	170.2 ± 4.15	210.9 ± 8.52	98.23 ± 1.23	97.63 ± 2.41	91.36 ± 2.54
7	3.0	$AGLY_0$	128.1 ± 4.69	175.3 ± 7.96	260.4 ± 9.82	95.29 ± 1.47	91.85 ± 3.54	84.31 ± 2.32
		$AGLY_{30}$	165.9 ± 2.95	173.6 ± 4.31	226.2 ± 7.62	97.53 ± 1.85	97.25 ± 2.78	88.36 ± 1.85

(n=3, ±S.D.)

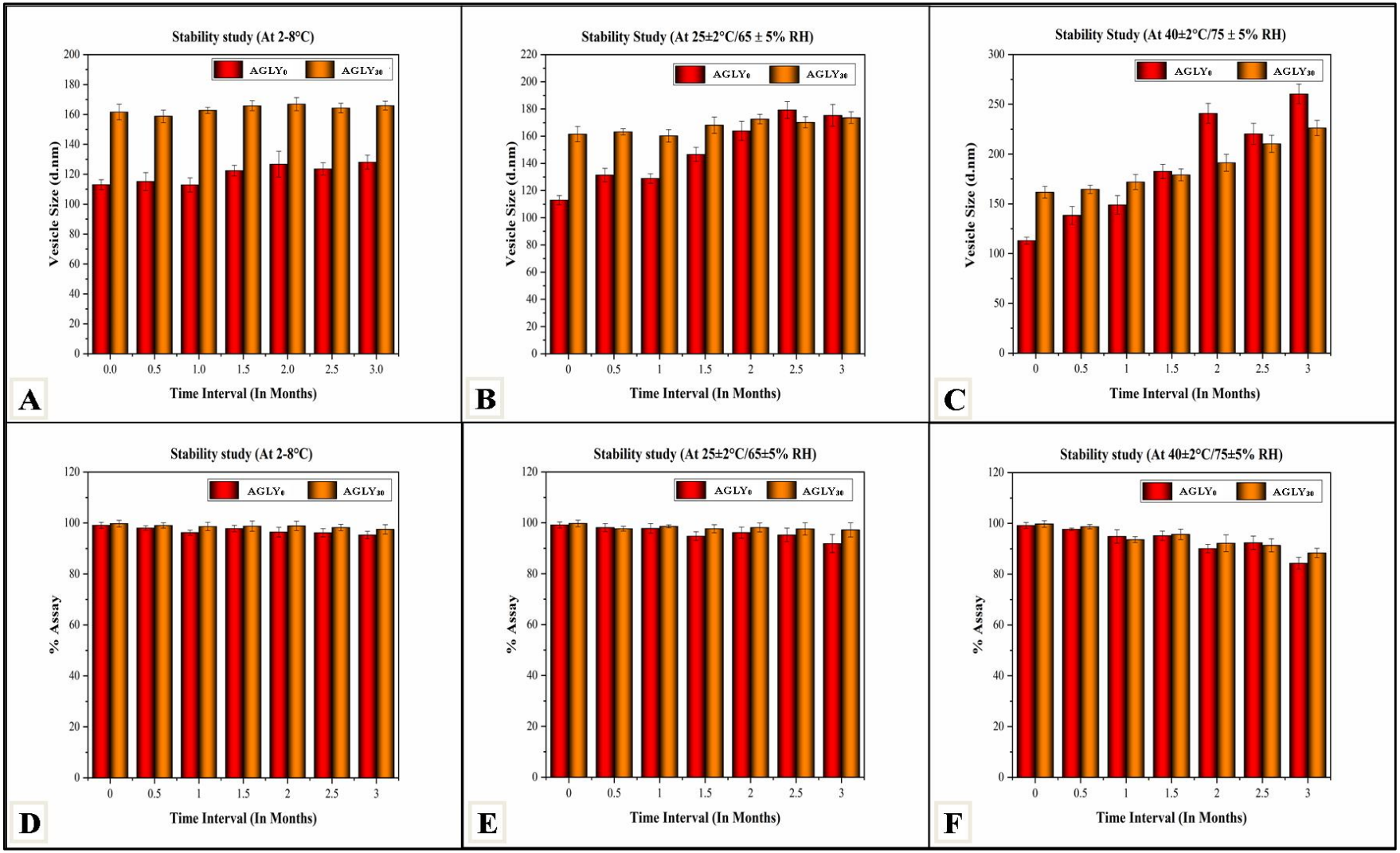

Figure- 5.23. Stability study of ATO loaded glycerosomes ($AGLY_{30}$) and ATO loaded liposomes ($AGLY_0$) at different storage condition

Chapter 5 – ATO loaded Glycerosomes

5.28. References:

1. Salem, H.F., et al., *Formulation design and optimization of novel soft glycerosomes for enhanced topical delivery of celecoxib and cupferron by Box–Behnken statistical design.* Drug development and industrial pharmacy, 2018. **44**(11): p. 1871-1884.
2. Manca, M.L., et al., *Close-packed vesicles for diclofenac skin delivery and fibroblast targeting.* 2013. **111**: p. 609-617.
3. Zhang, K., et al., *Essential oil-mediated glycerosomes increase transdermal paeoniflorin delivery: Optimization, characterization, and evaluation In vitro and in vivo.* International journal of nanomedicine, 2017. **12**: p. 3521.
4. Manca, M.L., et al., *Improvement of quercetin protective effect against oxidative stress skin damages by incorporation in nanovesicles.* Colloids and Surfaces B: Biointerfaces, 2014. **123**: p. 566-574.
5. Manca, M.L., et al., *Glycerosomes: Investigation of role of 1, 2-dimyristoyl-sn-glycero-3-phosphatidycholine (DMPC) on the assembling and skin delivery performances.* International Journal of Pharmaceutics, 2017. **532**(1): p. 401-407.
6. Zhang, K., et al., *Preparation, characterization, and in vivo pharmacokinetics of nanostructured lipid carriers loaded with oleanolic acid and gentiopicrin.* International journal of nanomedicine, 2013. **8**: p. 3227.
7. He, Y., et al., *Influence of probe-sonication process on drug entrapment efficiency of liposomes loaded with a hydrophobic drug.* International Journal of Polymeric Materials and Polymeric Biomaterials, 2019. **68**(4): p. 193-197.
8. Duangjit, S., et al., *Characterization and In vitro skin permeation of meloxicam-loaded liposomes versus transfersomes.* Journal of drug delivery, 2011. **2011**.
9. Moolakkadath, T., et al., *Preparation and optimization of fisetin loaded glycerol based soft nanovesicles by Box-Behnken design.* International Journal of Pharmaceutics, 2020. **578**: p. 119125.

10. Han, E.-J., A.-H. Chung, and I.-J. Oh, *Analysis of residual solvents in poly (lactide-co-glycolide) nanoparticles.* Journal of Pharmaceutical Investigation, 2012. **42**(5): p. 251-256.

11. Yang, Y., X.Y. Xie, and X.G. Mei, *Preparation and In vitro evaluation of thienorphine-loaded PLGA nanoparticles.* Drug delivery, 2016. **23**(3): p. 777-783.

12. Grodowska, K. and A. Parczewski, *Analytical methods for residual solvents determination in pharmaceutical products.* Acta Poloniae Pharmaceutica. Drug Research, 2010. **67**(1).

13. Manca, M.L., et al., *Glycerosomes: Investigation of role of 1, 2-dimyristoyl-sn-glycero-3-phosphatidycholine (DMPC) on the assembling and skin delivery performances.* 2017. **532**(1): p. 401-407.

14. Manca, M.L., et al., *Glycerosomes: Use of hydrogenated soy phosphatidylcholine mixture and its effect on vesicle features and diclofenac skin penetration.* International journal of pharmaceutics, 2016. **511**(1): p. 198-204.

15. Innes, A., et al., *Complement activation by cellulosic dialysis membranes.* 1994. **47**(2): p. 155-158.

16. Melchior, P., et al., *Complement activation by dialysis membranes and its association with secondary membrane formation and surface charge.* 2021. **45**(7): p. 770-778.

17. Xie, Y., et al., *Atorvastatin-loaded micelles with bone-targeted ligand for the treatment of osteoporosis.* Drug Delivery, 2017. **24**(1): p. 1067-1076.

18. AlKhani, M., A. Al-Laham, and M.A. Al-Mardini, *Simultaneous and precise HPLC method for quantification of atorvastatin in rat plasma and intestinal perfusion solution.* Int J Pharm Sci Rev Res, 2016. **38**(2): p. 70-4.

19. Jain, A., S.K.J.C. Jain, and p.o. lipids, *In vitro release kinetics model fitting of liposomes: An insight.* 2016. **201**: p. 28-40.

20. Ramteke, K., et al., *Mathematical models of drug dissolution: a review*. 2014. **3**(5): p. 388-396.

21. Trucillo, P.J.P., *Drug carriers: A review on the most used mathematical models for drug release.* 2022. **10**(6): p. 1094.

22. Siepmann, J. and F.J.I.j.o.p. Siepmann, *Mathematical modeling of drug release from lipid dosage forms.* 2011. **418**(1): p. 42-53.

23. Babu, R., et al., *The influence of various methods of cold storage of skin on the permeation of melatonin and nimesulide.* 2003. **86**(1): p. 49-57.

24. De, A., M. Mathur, and M.J.I.J.o.M.R. Gore, *Viability of cadaver skin grafts stored in skin bank at two different temperatures.* 2008. **128**(6): p. 769-771.

25. Mahmoud, M.O., et al., *Transdermal delivery of atorvastatin calcium from novel nanovesicular systems using polyethylene glycol fatty acid esters: ameliorated effect without liver toxicity in poloxamer 407-induced hyperlipidemic rats.* Journal of controlled release, 2017. **254**: p. 10-22.

26. Wavikar, P. and P.J.A.p. Vavia, *Nanolipidgel for enhanced skin deposition and improved antifungal activity.* 2013. **14**: p. 222-233.

27. Kim, H., et al., *Characteristics of skin deposition of itraconazole solubilized in cream formulation.* 2019. **11**(4): p. 195.

28. Elshall, A.A., et al., *Ex vivo permeation parameters and skin deposition of melatonin-loaded microemulsion for treatment of alopecia.* 2022. **8**(1): p. 28.

29. Chen, M., X. Liu, and A.J.I.j.o.p. Fahr, *Skin penetration and deposition of carboxyfluorescein and temoporfin from different lipid vesicular systems: In vitro study with finite and infinite dosage application.* 2011. **408**(1-2): p. 223-234.

30. Aboud, H.M., et al., *Development, optimization, and evaluation of carvedilol-loaded solid lipid nanoparticles for intranasal drug delivery.* AAPS pharmscitech, 2016. **17**(6): p. 1353-1365.

31. Segeritz, C.-P. and L. Vallier, *Cell culture: Growing cells as model systems In vitro*, in *Basic science methods for clinical researchers*. 2017, Elsevier. p. 151-172.

32. Helgason, C.D. and C.L. Miller, *Basic cell culture protocols*. 2005: Totowa, NJ.: Humana Press.

33. Tripathi, B.D. and N. Singh, *Wound Healing Potential of Transdermal Patches Containing Bioactive Fraction: A Novel Approach.* International Journal of Pharmacy & Life Sciences, 2020. **11**(7): p. 83-83.

34. Shah, P., et al., *In vitro assessment of acyclovir permeation across cell monolayers in the presence of absorption enhancers.* Drug development and industrial pharmacy, 2008. **34**(3): p. 279-288.

35. Chen, S., R. Einspanier, and J. Schoen, *Transepithelial electrical resistance (TEER): a functional parameter to monitor the quality of oviduct epithelial cells cultured on filter supports.* Histochemistry and cell biology, 2015. **144**(5): p. 509-515.

36. Poenar, D.P., et al., *Low-cost method and biochip for measuring the trans-epithelial electrical resistance (TEER) of esophageal epithelium.* Materials, 2020. **13**(10): p. 2354.

37. Rani, D., et al., *Formulation development and in-vitro evaluation of minoxidil bearing glycerosomes.* Am. J. Biomed. Res, 2016. **4**: p. 27-37.

38. Yamaguchi, T., et al., *Effects of frequency and power of ultrasound on the size reduction of liposome.* 2009. **160**(1): p. 58-62.

39. He, Y., et al., *Influence of probe-sonication process on drug entrapment efficiency of liposomes loaded with a hydrophobic drug.* 2019. **68**(4): p. 193-197.

40. Lee, Y. and D.H. Thompson, *Stimuli-responsive liposomes for drug delivery.* Wiley Interdiscip Rev Nanomed Nanobiotechnol, 2017. **9**(5).

41. Gonzalez Gomez, A., et al., *Liposomal Nanovesicles for Efficient Encapsulation of Staphylococcal Antibiotics.* ACS Omega, 2019. **4**(6): p. 10866-10876.

42. Salem, H.F., et al., *Formulation design and optimization of novel soft glycerosomes for enhanced topical delivery of celecoxib and cupferron by Box–Behnken statistical design.* 2018. **44**(11): p. 1871-1884.

43. Salem, H.F., et al., *Glycerosomal thermosensitive in situ gel of duloxetine HCl as a novel nanoplatform for rectal delivery: In vitro optimization and in vivo appraisal.* 2022. **12**(12): p. 3083-3103.

44. Sangshetti, J.N., et al., *Quality by design approach: Regulatory need.* Arabian Journal of Chemistry, 2017. **10**: p. S3412-S3425.

45. Vining, G.J.Q.E., *Technical advice: residual plots to check assumptions.* 2010. **23**(1): p. 105-110.

46. Naguib, M.J., et al., *Investigating the potential of utilizing glycerosomes as a novel vesicular platform for enhancing intranasal delivery of lacidipine.* International Journal of Pharmaceutics, 2020. **582**: p. 119302.

47. Essa, E.A.J.A.J.o.P., *Effect of formulation and processing variables on the particle size of sorbitan monopalmitate niosomes.* 2010. **4**(4).

48. Yamaguchi, T., et al., *Effects of frequency and power of ultrasound on the size reduction of liposome.* Chemistry and physics of lipids, 2009. **160**(1): p. 58-62.

49. Hong, S.-S. and S.-J.J.J.o.P.I. Lim, *Laboratory scale production of injectable liposomes by using cell disruptor to avoid the probe sonication process.* 2015. **45**: p. 73-78.

50. Salem, H.F., et al., *A novel transdermal nanoethosomal gel of lercanidipine HCl for treatment of hypertension: optimization using Box-Benkhen design, In vitro and in vivo characterization.* 2020. **10**: p. 227-240.

51. Moolakkadath, T., et al., *Preparation and optimization of fisetin loaded glycerol based soft nanovesicles by Box-Behnken design.* 2020. **578**: p. 119125.

52. Zhang, K., et al., *Essential oil-mediated glycerosomes increase transdermal paeoniflorin delivery: Optimization, characterization, and evaluation In vitro and in vivo.* 2017. **12**: p. 3521.

53. Hosny, K.M., et al., *Nanovesicular systems loaded with a recently approved second generation type-5 phospodiesterase inhibitor (avanafil): I. Plackett-Burman screening and characterization.* 2018. **43**: p. 154-159.

54. Li, F., et al., *Preparation and evaluation of lyophilized liposome-encapsulated bufadienolides.* 2009. **35**(9): p. 1048-1058.

55. Sinico, C., et al., *Liposomes as carriers for dermal delivery of tretinoin: In vitro evaluation of drug permeation and vesicle–skin interaction.* Journal of Controlled Release, 2005. **103**(1): p. 123-136.

56. Manca, M.L., et al., *Improvement of quercetin protective effect against oxidative stress skin damages by incorporation in nanovesicles.* 2014. **123**: p. 566-574.

57. Naguib, M.J., Y.R. Hassan, and W.H. Abd-Elsalam, *3D printed ocusert laden with ultra-fluidic glycerosomes of ganciclovir for the management of ocular cytomegalovirus retinitis.* International Journal of Pharmaceutics, 2021. **607**: p. 121010.

58. Manca, M.L., et al., *Glycerosomes: A new tool for effective dermal and transdermal drug delivery.* 2013. **455**(1-2): p. 66-74.

59. Gupta, V., P.J.J.o.d.d.s. Trivedi, and technology, *Enhancement of storage stability of cisplatin-loaded protransfersome topical drug delivery system by surface modification with block copolymer and gelling agent.* 2012. **22**(4): p. 361-366.

60. Jain, A.K., et al., *Adapalene loaded solid lipid nanoparticles gel: an effective approach for acne treatment.* 2014. **121**: p. 222-229.

61. Gyanewali, S., et al., *Formulation development and In vitro–in vivo assessment of protransfersomal gel of anti-resorptive drug in osteoporosis treatment.* International Journal of Pharmaceutics, 2021. **608**: p. 121060.

62. Abdellatif, M.M., I.A. Khalil, and M.A.J.I.j.o.p. Khalil, *Sertaconazole nitrate loaded nanovesicular systems for targeting skin fungal infection: in-vitro, ex-vivo and in-vivo evaluation.* 2017. **527**(1-2): p. 1-11.

63. Manconi, M., et al., *Development and characterization of liposomes containing glycols as carriers for diclofenac.* 2009. **342**(1-3): p. 53-58.

64. Naguib, M.J., Y.R. Hassan, and W.H.J.I.J.o.P. Abd-Elsalam, *3D printed ocusert laden with ultra-fluidic glycerosomes of ganciclovir for the management of ocular cytomegalovirus retinitis.* 2021. **607**: p. 121010.

65. Manca, M.L., et al., *Glycerosomes: Use of hydrogenated soy phosphatidylcholine mixture and its effect on vesicle features and diclofenac skin penetration.* 2016. **511**(1): p. 198-204.